MIT Open Access Articles

A parameterized-background data-weak approach to variational data assimilation: formulation, analysis, and application to acoustics

Massachusetts Institute of Technology

DSpace@MIT

A Parametrized-Background Data-Weak Approach to Variational Data Assimilation: Formulation, Analysis, and Application to Acoustics

Yvon Maday[2], Anthony T Patera[1], James D Penn[1], and Masayuki Yano[1*]

[1] *Department of Mechanical Engineering, Massachusetts Institute of Technology, 77 Massachusetts Avenue, Cambridge, MA 02139, USA*
[2] *Laboratoire Jacques-Louis Lions, Université Pierre et Marie Curie, 4 Place Jussieu, 75005 Paris, France*

SUMMARY

We present a Parametrized-Background Data-Weak (PBDW) formulation of the variational data assimilation (state estimation) problem for systems modeled by partial differential equations. The main contributions are a constrained optimization weak framework informed by the notion of experimentally observable spaces; *a priori* and *a posteriori* error estimates for the field and associated linear-functional outputs; Weak Greedy construction of prior (background) spaces associated with an underlying potentially high–dimensional parametric manifold; stability-informed choice of observation functionals and related sensor locations; and finally, output prediction from the optimality saddle in $\mathcal{O}(M^3)$ operations, where M is the number of experimental observations. We present results for a synthetic Helmholtz acoustics model problem to illustrate the elements of the methodology and confirm the numerical properties suggested by the theory. To conclude, we consider a physical raised-box acoustic resonator chamber: we integrate the PBDW methodology and a Robotic Observation Platform to achieve real-time *in situ* state estimation of the time-harmonic pressure field; we demonstrate the considerable improvement in prediction provided by the integration of a best-knowledge model and experimental observations; we extract even from these results with real data the numerical trends indicated by the theoretical convergence and stability analyses.
Copyright © 0000 John Wiley & Sons, Ltd.

1. INTRODUCTION

The best–knowledge mathematical model of a physical system is often deficient due to limitations imposed by available knowledge, calibration requirements, and computational solution costs. Accurate prediction thus requires the incorporation of experimental observations in particular to accommodate both anticipated, or parametric, uncertainty as well as unanticipated, or nonparametric, uncertainty. We present in this paper a Parametrized-Background Data-Weak (PBDW) formulation of the variational data assimilation problem for physical systems modeled by partial differential equations (PDEs).

Our goal is state estimation. We seek an approximation, $u^*_{\cdot,\cdot}$, to the true field u^{true}, over some spatial domain of interest, Ω. (The state estimate subscript placeholders anticipate two

---

*Correspondence to: 77 Massachusetts Ave, Rm 3-237, Cambridge, MA 02139. E-mail: myano@mit.edu

*Prepared using **nmeauth.cls** [Version: 2010/05/13 v3.00]*

discretization parameters to be introduced shortly.) We shall afford ourselves two sources of information: a best-knowledge (bk) mathematical model in the form of a parametrized PDE defined over Ω (or more generally a domain Ω^{bk} which includes Ω); M experimental observations of the true field, interpreted as the application of prescribed observation functionals [10] ℓ^{o}_m, $m = 1, \ldots, M$, to u^{true}. We shall assume that the true field is deterministic and time-independent (or time-harmonic); we shall further assume, in this first paper, that the observations are noise-free.

Given a parameter value μ in a prescribed parameter domain $\mathcal{D}$ we denote the solution to our best-knowledge parametrized PDE as $u^{\text{bk},\mu}$. We may then introduce the parametric manifold associated with our best-knowledge model as $\mathcal{M}^{\text{bk}} \equiv \{u^{\text{bk},\mu} | \mu \in \mathcal{D}\}$. We intend, but we shall not assume, that u^{true} is close to the manifold: these exists a $\tilde{\mu} \in \mathcal{D}$ such that u^{true} is well approximated by $u^{\text{bk},\tilde{\mu}}$. We shall require that, *in any event*, our state estimate $u^*_{\cdot,\cdot}$, now denoted $u^*_{\cdot,M}$, shall converge to u^{true} in the limit of many (noise-free) observations, $M \to \infty$.

To provide a more concrete point of reference, we instantiate the terms introduced above for the problem we shall consider in this paper. The physical system is a raised-box acoustic resonator chamber: the state we wish to estimate is the time-harmonic (complex) pressure field; the domain of interest Ω is the interior of the raised box, or resonator chamber; the observation functionals are averages over the face of a microphone placed at different positions $x^{\text{c}}_m \in \Omega$, $m = 1, \ldots, M$. The best-knowledge model is the Helmholtz PDE of acoustics: the domain Ω^{bk} is a large hemispherical dome which includes Ω; the boundary conditions comprise a speaker Neumann model as well as farfield radiation; the (here, singleton) parameter μ, which appears in the PDE and boundary conditions, is the wavenumber (or nondimensional frequency) of the time-harmonic pressure; the parameter domain $\mathcal{D} = [0.5, 1.0]$ (roughly 1000 Hz to 2000 Hz in dimensional terms).

We shall first motivate the PBDW formulation from a perspective directly relevant to the theme of this special issue, model order reduction. For concreteness, we consider the particular model-reduction approach which we shall subsequently pursue in this particular paper, the certified reduced basis (CRB) method; however, other approaches are also possible and are briefly summarized below. In this context, the point of departure is the parametric manifold $\mathcal{M}^{\text{bk}}$ associated with the solutions of our best-knowledge PDE. (The CRB approach requires for computational expediency that the parametrized PDE be affine in functions of the parameter: often inspection suffices to verify this condition; more generally, the Empirical Interpolation Method [2] provides an (approximate) construction.) We shall then revisit the PBDW formulation but now from the related perspectives of data interpolation, least-squares approximation, and variational data assimilation. In this context, the point of departure is the minimization of the misfit between model predictions and experimental observations.

We briefly summarize the ingredients of the CRB approach [25]: construction of a Lagrange [23] approximation space $\mathcal{Z}_N$ as the span of N snapshots, $\hat{\mu}_n \in \mathcal{D} \to u^{\text{bk},\hat{\mu}_n}$, $n = 1, \ldots, N$, on the parametric manifold $\mathcal{M}^{\text{bk}}$; approximation of the solution of the PDE, $u^{\text{bk},\mu}$ for any parameter value $\mu \in \mathcal{D}$, as the Galerkin projection over $\mathcal{Z}_N$, $u^{\text{bk},\mu}_N$; development of *a posteriori* error estimates $\Delta^{\text{bk},\mu}_N$ — in fact, often *bounds* — for the error $\|u^{\text{bk},\mu} - u^{\text{bk},\mu}_N\|$ in terms of the dual norm of the residual and corresponding stability constants; formulation of Construction-Evaluation procedures which permit rapid computation of the CRB approximation and *a posteriori* error bound in the limit of many queries $\mu \to u^{\text{bk},\mu}_N, \Delta^{\text{bk},\mu}_N$; application of Weak Greedy sampling procedures which exploit the Construction-Evaluation procedure to efficiently identify quasi-optimal (snapshots and hence) approximation spaces $\mathcal{Z}_N$ relative to the Kolmogorov gold standard [3]; and finally, deployment in an Offline–Online computational framework such that the Online stage — the response to each new parameter request — invokes only inexpensive Evaluations. The method is relevant in the real-time context or the many-query context in which the Offline (and Construction) costs are respectively irrelevant or amortized.

We now turn to real physical systems, for example the raised-box acoustic resonator which we shall study in the concluding section of this paper. For such a physical system

and associated best-knowledge model, we may propose to approximate u^{true} by $u_N^{\text{bk},\tilde{\mu}}$, the CRB approximation of the closest element on the best-knowledge manifold $\mathcal{M}^{\text{bk}}$. We identify two impediments. First, in general we will not know $\tilde{\mu}$ *a priori*: (anticipated) parametric uncertainty may arise for example due to imperfect control of ambient temperature and thus sound speed. Hence we cannot instantiate our weak form and as a result we are simply not able to apply Galerkin projection to determine $u_N^{\text{bk},\tilde{\mu}}$. Second, we cannot control the *model* error $\inf_{\tilde{\mu} \in \mathcal{D}} \|u^{\text{true}} - u^{\text{bk},\tilde{\mu}}\|$: unanticipated nonparametric uncertainty may arise for example due to uncharacterized impedances on the walls of the resonator chamber. In short, CRB approximation assumes, often quite unrealistically, that our best-knowledge mathematical model reflects complete knowledge of the physical system.

Data can provide the necessary closure for both the parametric and nonparametric sources of uncertainty. In particular, we first write our state estimate $u_{N,M}^*$ as the sum of two contributions, $u_{N,M}^* \equiv z_{N,M}^* + \eta_{N,M}^*$. The first contribution to $u_{N,M}^*$, $z_{N,M}^* \in \mathcal{Z}_N$, is the "deduced background estimate" which represents anticipated uncertainty; $\mathcal{Z}_N$ is now interpreted as a background or prior space which approximates the best-knowledge manifold on which we hope the true state resides. As already discussed, non-zero model error is a virtual certainty, and thus we cannot realistically assume that u^{true} lies exactly on our best-knowledge manifold, which thus motivates the second contribution to $u_{N,M}^*$. This second contribution to $u_{N,M}^*$, $\eta_{N,M}^* \in \mathcal{U}_M$, is the "update estimate" which accommodates unanticipated uncertainty; $\mathcal{U}_M$ is the span of the Riesz representations of our M observation functionals [28]. We then search for $\eta_{N,M}^*$ of minimum norm — we look for the smallest correction to the best-knowledge parametric manifold — subject to the observation constraints $\ell_m^o(u^{\text{true}}) = \ell_m^o(u_{N,M}^*)$, $m = 1, \ldots, M$. In conclusion, the data effects the projection onto $\mathcal{Z}_N$ — in effect serving as test space — and furthermore supplements the best-knowledge model — thus also serving as a supplemental trial space.

The prior or background space $\mathcal{Z}_N$ may be generated from the manifold $\mathcal{M}^{\text{bk}}$ by a variety of model-order reduction approaches. We may consider Weak Greedy procedures as developed in the reduced basis context and summarized above in our discussion of the principal CRB ingredients. We may consider classical Proper Orthogonal Decomposition (POD) [14]; POD is, relative to Weak Greedy, more readily implemented, more optimal, but also considerably less efficient in the Offline stage. We may consider Taylor spaces [9] and Hermite spaces [12]: expansion of the best-knowledge solution about one or several nominal parameter values in $\mathcal{D}$ — in effect, higher order tangent approximations of the parametric manifold. Finally, and under more restrictive hypotheses, we may also consider "Superposition" [6, 5]: $\mathcal{Z}_N$ is constructed as the span of exact homogeneous solutions to our best-knowledge PDE additionally parametrized by an appropriate truncated representation of the trace over $\partial\Omega$.

We can now relate this PBDW approach to a variety of existing methods. We first consider the model-reduction perspective: PBDW is an approximation method that seeks solution in the reduced-basis space $\mathcal{Z}_N \oplus \mathcal{U}_M$ based on projection-by-data, as opposed to projection-by-model in the standard reduced basis method. We next consider the data interpolation perspective: PBDW reduces to the Generalized Empirical Interpolation Method (GEIM) [18, 22, 21] for $N = M$, any given $\mathcal{Z}_N$; PBDW reduces to Gappy-POD [8, 27] for $M \geq N$, $\mathcal{Z}_N$ generated by a Proper Orthogonal Decomposition (POD), and $u_{N,M}^* \equiv z_{N,M}^*$ (no update correction). We then continue with the least-squares perspective: PBDW reduces to the Stable Least Squares Approximation [6] for $M \geq N$, $\mathcal{Z}_N$ chosen by Superposition, and $u_{N,M}^* \equiv z_{N,M}^*$ (no update correction); PBDW may also be interpreted, albeit less directly, as linearized Structured Total Least Squares [20] for $M \geq N$, $\mathcal{Z}_N$ chosen by Taylor expansion. Finally, and most importantly, PBDW is a *special case* of 3D-VAR variational data assimilation [17] for a parametrized background and a particular choice of (penalized-update) background covariance[†]; note that in the noise-free case considered in this paper, the variational data assimilation optimization

---

[†]It thus follows, by association, that the PBDW formulation can be related to filtering approaches [16, 13].

reduces to a constrained estimation problem. We emphasize that PBDW is not a generalization of 3D-VAR, but rather a particular choice for the 3D-VAR constituents.

The PBDW formulation does provide some new contributions:

1. Our constrained optimization weak framework is informed by the notion of experimentally observable spaces [28] — our update spaces $\mathcal{U}_M$ — which in turn allows us to incorporate and analyze data within the standard variational setting for PDEs [24]: we can thus develop *a priori* error bounds and *a posteriori* error estimates for the field and associated linear-functional "quantity-of-interest" outputs as a function of N, the dimension of the background space, and M, the number of experimental observations.

2. The *a priori* theory can serve to inform strategies for the efficient identification of optimal observations functionals — and hence (for localized observation functionals) optimal sensor placement. Different optimality criteria may be considered. In this paper we choose as criterion the stability of the deduced background estimate $z^*_{N,M}$. Our methods are thus related to classical Design-of-Experiment approaches [11], however with an emphasis on state estimation rather than parameter estimation; in particular both methods rely on singular-value considerations. We may also consider criteria which balance stability of the background estimate $z^*_{N,M}$ with accuracy of the update estimate $\eta^*_{N,M}$ [26].

3. We incorporate several important aspects of model-order reduction: efficient Weak Greedy construction of rapidly convergent prior (background) spaces associated with an underlying potentially high–dimensional parametric manifold; output prediction from the optimality saddle in $\mathcal{O}((N+M)^3)$ operations for N and M anticipated small. (We note that stability will require $M \geq N$: a good background space thus reduces not only computational effort but also experimental cost.)

4. The PBDW formulation offers simplicity and generality: the best-knowledge model appears only in the Offline stage, and solely in the generation of the space $\mathcal{Z}_N$.

These features will be highlighted in the sections that follow.

We note that projection-by-data — a problem in approximation theory — rather than projection-by-model — a problem in PDE discretization — also has many advantages with respect to the mathematical theory. Projection-by-data can largely eliminate many of the standard requirements of projection-by-model in particular related to boundary conditions and initial conditions; for example, the domain over which we reconstruct the state, Ω, can be a subset of the best-knowledge spatial domain, Ω^{bk}, and indeed Ω can even be a low dimensional manifold in Ω^{bk}. Even more ambitiously, in projection-by-data we can accommodate norms which may be considerably stronger than the norms required for well-posedness in projection-by-model; furthermore, the greater regularity required by data in these stronger norms can be justified by the application of temporal or spatial filters — in short, by a re-definition of the true field, u^{true}. In subsequent studies, we shall explore further these theoretical generalizations and associated computational extensions and improvements.

We emphasize that in this paper we restrict ourselves to state estimation: the PBDW formulation chooses a best state estimate from $\mathcal{Z}_N$ and $\mathcal{U}_M$ as guided by the constrained minimization statement. Clearly in many cases state estimation can be related to parameter estimation [11] and source identification [1], however we do not here take the necessary steps to infer from our best state estimate $u^*_{N,M}$ a best parameter estimate $\mu^*_{N,M}$. In particular, in our current paper μ and $\mathcal{D}$ serve only in the (Offline) construction of $\mathcal{Z}_N$: the Online stage does not benefit from any prior on the parameter, nor does the Online stage provide any posterior for the parameter. However, we note that the PBDW update contribution suggests both a complication and an extension to current parameter estimation approaches: $\|\eta^*_{N,M}\|$ allows us to explore the sensitivity of any given parameter estimate to model error. We pursue this possibility in subsequent papers, in which we shall also consider noisy measurements — another important source of uncertainty in (state and) parameter estimation.

In Section 2, we present the PBDW formulation and associated numerical analysis. In Section 3, we present results for a synthetic Helmholtz problem: we illustrate the elements of the methodology; we confirm the numerical properties suggested by the theory. In Section 4, we present results for a physical raised-box acoustic resonator chamber: we integrate the PBDW methodology and a Robotic Observation Platform to achieve real-time *in situ* estimation of the full pressure field over the resonator chamber.

2. FORMULATION

2.1. Preliminaries

By way of preliminaries, we introduce notations used throughout this paper. We first introduce the standard $L^2(\Omega)$ Hilbert space over the domain $\Omega \subset \mathbb{R}^d$ endowed with an inner product $(w, v)_{L^2(\Omega)} \equiv \int_\Omega wv dx$ and the induced norm $\|w\|_{L^2(\Omega)} = \sqrt{(w,w)_{L^2(\Omega)}}$; $L^2(\Omega)$ consists of functions $\{w \mid \|w\|_{L^2(\Omega)} < \infty\}$. We next introduce the standard $H^1(\Omega)$ Hilbert space over Ω endowed with an inner product $(w, v)_{H^1(\Omega)} \equiv \int_\Omega \nabla w \cdot \nabla v dx + \int_\Omega wv dx$ and the induced norm $\|w\|_{H^1(\Omega)} \equiv \sqrt{(w,w)_{H^1(\Omega)}}$; $H^1(\Omega)$ consists of functions $\{w \mid \|w\|_{H^1(\Omega)} < \infty\}$. We also introduce the $H_0^1(\Omega)$ Hilbert space over Ω endowed with the $H^1(\Omega)$ inner product and $H^1(\Omega)$ norm; $H_0^1(\Omega)$ consists of functions $\{w \in H^1(\Omega) \mid w|_{\partial\Omega} = 0\}$. We note that, for simplicity, we shall consider the formulation over real-valued field; however, in the subsequent applications that appear in Sections 3 and 4, we shall invoke corresponding extension to complex-valued fields.

We now introduce a Hilbert space $\mathcal{U}$ over Ω endowed with an inner product $(\cdot, \cdot)$ and the induced norm $\|w\| = \sqrt{(w,w)}$; $\mathcal{U}$ consists of functions $\{w \mid \|w\| < \infty\}$. We assume that $H_0^1(\Omega) \subset \mathcal{U} \subset H^1(\Omega)$. We denote the dual space of $\mathcal{U}$ by $\mathcal{U}'$ and the associated duality paring by $\langle \cdot, \cdot \rangle_{\mathcal{U}' \times \mathcal{U}}$. The Riesz operator $R_{\mathcal{U}} : \mathcal{U}' \to \mathcal{U}$ satisfies, for each $\ell \in \mathcal{U}'$, $(R_{\mathcal{U}} \ell, v) = \ell(v) \ \forall v \in \mathcal{U}$. For any subspace $\mathcal{Q} \subset \mathcal{U}$, the orthogonal projection operator $\Pi_{\mathcal{Q}} : \mathcal{U} \to \mathcal{Q}$ satisfies $(\Pi_{\mathcal{Q}} w, v) = (w, v) \ \forall v \in \mathcal{Q}$. The orthogonal complement of $\mathcal{Q}$ is given by $\mathcal{Q}^\perp \equiv \{w \in \mathcal{U} | (w, v) = 0 \ \forall v \in \mathcal{Q}\}$.

2.2. Unlimited-Observations Statement

We first introduce generic hierarchical background (or prior) spaces

$$\mathcal{Z}_1 \subset \mathcal{Z}_2 \subset \cdots \subset \mathcal{Z}_{N_{\max}} \subset \cdots \subset \mathcal{U};$$

here the last ellipsis indicates that although in practice we shall consider N at most $N_{\max}$, in principle we might extend the analysis to an infinite sequence of refinements. We intend, but not assume, that

$$\epsilon_N^{\mathrm{bk}}(u^{\mathrm{true}}) \equiv \inf_{w \in \mathcal{Z}_N} \|u^{\mathrm{true}} - w\| \leq \epsilon \quad \text{as} \quad N \to \infty$$

for ϵ an acceptable tolerance. As mentioned in the introduction, the background spaces may be generated from the best-knowledge manifold $\mathcal{M}^{\mathrm{bk}}$ by a variety of model reduction approaches; the spaces consist of candidate states realized by anticipated, and parametrized, uncertainty in the model. We consider several specific choices in detail in Section 2.7.2.

We are now ready to state the unlimited-observations PBDW minimization statement: find $(u_N^* \in \mathcal{U}, z_N^* \in \mathcal{Z}_N, \eta_N^* \in \mathcal{U})$ such that

$$(u_N^*, z_N^*, \eta_N^*) = \arg\inf_{\substack{u_N \in \mathcal{U} \\ z_N \in \mathcal{Z}_N \\ \eta_N \in \mathcal{U}}} \|\eta_N\|^2 \tag{1}$$

subject to

$$\begin{aligned} (u_N, v) &= (\eta_N, v) + (z_N, v) \quad \forall v \in \mathcal{U}, \\ (u_N, \phi) &= (u^{\mathrm{true}}, \phi) \quad \forall \phi \in \mathcal{U}. \end{aligned} \tag{2}$$

The following proposition summarizes the solution to the minimization problem.

Proposition 1. The solution to the PBDW minimization statement (1) is

$$u_N^* = u^{\text{true}}, \quad z_N^* = \Pi_{\mathcal{Z}_N} u^{\text{true}}, \quad \text{and} \quad \eta_N^* = \Pi_{\mathcal{Z}_N^\perp} u^{\text{true}}.$$

Proof
We first deduce from $(2)_2$ that $u_N^* = u^{\text{true}}$. We next deduce from $(2)_1$ that $\eta_N^* = u^{\text{true}} - z_N^*$. We then note that, since we wish to minimize $\|\eta_N^*\|$, we must choose $z_N^* = \Pi_{\mathcal{Z}_N} u^{\text{true}}$ such that $\eta_N^* = \Pi_{\mathcal{Z}_N^\perp} u^{\text{true}}$. □

Proposition 1 provides a precise interpretation for u_N^*, z_N^* and η_N^* and solidifies the interpretation alluded to in the introduction: $u_N^* \in \mathcal{U}$ is the "state estimate," which in fact is equal to the true state u^{true}; $z_N^* \in \mathcal{Z}_N$ is the "deduced background", the component of the state formed by the anticipated, and parametrized, uncertainty that lies in the background space $\mathcal{Z}_N$; $\eta_N^* \in \mathcal{Z}_N^\perp$ is the "update", the component of the state formed by unanticipated, and in some sense non-parametric, uncertainty that lies outside of the background space $\mathcal{Z}_N$. Note that the update η_N^* completes the deficient prior space such that $u^{\text{true}} = u_N^* = z_N^* + \eta_N^*$.

We now derive a (simplified) Euler-Lagrange equations associated with the PBDW minimization statement (1). Towards this end, we first introduce the Lagrangian,

$$\mathcal{L}(u_N, z_N, \eta_N, v, \phi) \equiv \frac{1}{2}\|\eta_N\|^2 + (u_N - \eta_N - z_N, v) + (u_N - u^{\text{true}}, \phi).$$

Here, $u_N \in \mathcal{U}$, $z_N \in \mathcal{Z}_N$, and $\eta_N \in \mathcal{U}$; $v \in \mathcal{U}$ and $\phi \in \mathcal{U}$ are the Lagrange multipliers. We then obtain the (full) Euler-Lagrange equations: find $(u_N^* \in \mathcal{U}, z_N^* \in \mathcal{Z}_N, \eta_N^* \in \mathcal{U}, v^* \in \mathcal{U}, \phi^* \in \mathcal{U})$ such that

$$\begin{aligned}
(v^*, \delta u) + (\phi^*, \delta u) &= 0 \quad \forall \delta u \in \mathcal{U}, \\
(v^*, \delta z) &= 0 \quad \forall \delta z \in \mathcal{Z}_N, \\
(\eta_N^*, \delta\eta) - (v^*, \delta\eta) &= 0 \quad \forall \delta\eta \in \mathcal{U}, \\
(u_N^* - \eta_N^* - z_N^*, \delta v) &= 0 \quad \forall \delta v \in \mathcal{U}, \\
(u_N^* - u^{\text{true}}, \delta\phi) &= 0 \quad \forall \delta\phi \in \mathcal{U}.
\end{aligned} \tag{3}$$

We readily obtain from $(3)_3$ and $(3)_1$ that $v^* = \eta_N^*$ and $\phi^* = v^* = -\eta_N^*$, respectively; we substitute η_N^* in place of v^* and $-\phi^*$. We in addition note from $(3)_5$ that $u_N = u^{\text{true}}$; we make the substitution to $(3)_4$. The substitutions yield the (simplified) Euler-Lagrange equation associated with the PBDW minimization statement (1): find $(\eta_N^* \in \mathcal{U}, z_N^* \in \mathcal{Z}_N)$ such that

$$\begin{aligned}
(\eta_N^*, q) + (z_N^*, q) &= (u^{\text{true}}, q) \quad \forall q \in \mathcal{U}, \\
(\eta_N^*, p) &= 0 \quad \forall p \in \mathcal{Z}_N,
\end{aligned} \tag{4}$$

and set $u_N^* = \eta_N^* + z_N^*$. We readily confirm the aforementioned background-update decomposition:

$$u_N^* = \eta_N^* + z_N^* = \Pi_{\mathcal{Z}_N^\perp} u^{\text{true}} + \Pi_{\mathcal{Z}_N} u^{\text{true}} = u^{\text{true}}.$$

We will primarily appeal to this saddle problem associated with the PBDW minimization statement to derive our data assimilation strategy and to develop associated theory.

2.3. Limited-Observations Statement

While the PBDW saddle statement (4) (or the minimization statement (1)) yields the exact state estimate $u_N^* = u^{\text{true}}$, the saddle statement is not actionable since the evaluation of $(u^{\text{true}}, q) \ \forall q \in \mathcal{U}$ in $(4)_1$ (or $(2)_2$) requires the full knowledge of the true state u^{true}. We wish

to devise an actionable statement that approximates the solution using a finite number of observations.

Towards this end, we introduce observation functionals

$$\ell_m^{\mathrm{o}} \in \mathcal{U}', \quad m = 1, \ldots, M_{\max},$$

such that the m-th perfect experimental observation is modeled as $\ell_m^{\mathrm{o}}(u^{\mathrm{true}})$. In other words, the functionals model the particular transducer used in data acquisition. For instance, if the transducer measures a local state value, we may model the transducer by a Gaussian convolution

$$\ell_m^{\mathrm{o}}(v) = \mathrm{Gauss}(v; x_m^{\mathrm{c}}, r_m),$$

where x_m^{c} is the center of the Gaussian that reflects the transducer location, and r_m is the standard deviation of the Gaussian that reflects the filter width of the transducer. We note observation functionals can be quite general and in fact are only limited by the capabilities of the associated transducers. Observation functionals may be either more global or more localized; in this paper, we restrict ourselves to "pointwise" measurements, which we model — for experimental and mathematical reasons[‡] — as local Gaussian convolutions. We in addition note that the precise form of the filter may not be important in cases for which the variation in the field occurs over scales much larger than r_m.

We then introduce *experimentally observable* update spaces. Namely, we consider hierarchical spaces

$$\mathcal{U}_M = \mathrm{span}\{q_m \equiv R_{\mathcal{U}}\ell_m^{\mathrm{o}}\}_{m=1}^M, \quad M = 1, \ldots, M_{\max}, \ldots;$$

here again the last ellipsis indicates that although in practice we shall consider M at most $M_{\max}$, in principle we might extend the analysis to an infinite sequence of refinements. We recall that $R_{\mathcal{U}}\ell \in \mathcal{U}$ is the Riesz representation of $\ell \in \mathcal{U}'$. Then, for $q_m = R_{\mathcal{U}}\ell_m^{\mathrm{o}} \in \mathcal{U}_M$,

$$(u^{\mathrm{true}}, q_m) = (u^{\mathrm{true}}, R_{\mathcal{U}}\ell_m^{\mathrm{o}}) = \ell_m^{\mathrm{o}}(u^{\mathrm{true}})$$

is an experimental observation associated with the m-th transducer. It follows that, for any $q \in \mathcal{U}_M$, $(u^{\mathrm{true}}, q) = (u^{\mathrm{true}}, \sum_{m=1}^M \alpha_m q_m) = \sum_{m=1}^M \alpha_m \ell_m^{\mathrm{o}}(u^{\mathrm{true}})$; hence (u^{true}, q) is a weighted sum of experimental observations. We say that $\mathcal{U}_M$ is *experimentally observable*.

We can now readily state our limited-observations PBDW minimization statement: find $(u_{N,M}^* \in \mathcal{U}, z_{N,M}^* \in \mathcal{Z}_N, \eta_{N,M}^* \in \mathcal{U})$ such that

$$(u_{N,M}^*, z_{N,M}^*, \eta_{N,M}^*) = \mathop{\arg\inf}_{\substack{u_{N,M} \in \mathcal{U} \\ z_{N,M} \in \mathcal{Z}_N \\ \eta_{N,M} \in \mathcal{U}}} \|\eta_{N,M}\|^2 \tag{5}$$

subject to

$$(u_{N,M}, v) = (\eta_{N,M}, v) + (z_{N,M}, v) \quad \forall v \in \mathcal{U},$$
$$(u_{N,M}, \phi) = (u^{\mathrm{true}}, \phi) \quad \forall \phi \in \mathcal{U}_M. \tag{6}$$

We arrive at the limited-observations minimization statement (5) from the unlimited-observations minimization statement (1) through a restriction of the test space for $(2)_2$ to $\mathcal{U}_M$. With this restriction, the right-hand side of the $(6)_2$, $(u^{\mathrm{true}}, \phi) \; \forall \phi \in \mathcal{U}_M$, is evaluated from the experimental observations.

[‡]Mathematically, the point-wise value is in general ill-defined for functions in $\mathcal{U} \supset H_0^1(\Omega \subset \mathbb{R}^d)$, $d > 1$. Practically, any physical transducer has a finite filter width.

We now derive a (simplified) Euler-Lagrange equations associated with the limited-observations PBDW minimization statement (5). Following the construction for the unlimited-observations case, we first introduce the Lagrangian

$$\mathcal{L}(u_{N,M}, z_{N,M}, \eta_{N,M}, v, \phi_M) \equiv \frac{1}{2}\|\eta_{N,M}\|^2 + (u_{N,M} - \eta_{N,M} - z_{N,M}, v) + (u_{N,M} - u^{\text{true}}, \phi_M);$$

here $u_{N,M} \in \mathcal{U}$, $z_{N,M} \in \mathcal{Z}_N$, $\eta_{N,M} \in \mathcal{U}$, $v \in \mathcal{U}$, and $\phi_M \in \mathcal{U}_M$. We then obtain the (full) Euler-Lagrange equations: find $(u_{N,M}^* \in \mathcal{U}, z_{N,M}^* \in \mathcal{Z}_N, \eta_{N,M}^* \in \mathcal{U}, v^* \in \mathcal{U}, \phi^* \in \mathcal{U}_M)$ such that

$$
\begin{aligned}
(v^*, \delta u) + (\phi^*, \delta u) &= 0 \quad \forall \delta u \in \mathcal{U}, \\
(v^*, \delta z) &= 0 \quad \forall \delta z \in \mathcal{Z}_N, \\
(\eta_{N,M}^*, \delta\eta) - (v^*, \delta\eta) &= 0 \quad \forall \delta\eta \in \mathcal{U}, \\
(u_{N,M}^* - \eta_{N,M}^* - z_{N,M}^*, \delta v) &= 0 \quad \forall \delta v \in \mathcal{U}, \\
(u_{N,M}^* - u^{\text{true}}, \delta\phi) &= 0 \quad \forall \delta\phi \in \mathcal{U}_M.
\end{aligned}
\tag{7}
$$

We now wish to simplify the statement. We first obtain from $(7)_1$ that $v^* = -\phi^*$; since $\phi^* \in \mathcal{U}_M$, we conclude that $v^* \in \mathcal{U}_M$. We then obtain from $(7)_3$ that $\eta_{N,M}^* = v^* = -\phi^*$; we again conclude that $\eta_{N,M}^* \in \mathcal{U}_M$. We now eliminate v^* (and ϕ^*) and rewrite $(7)_2$ as $(\eta_{N,M}^*, \delta z) = 0 \; \delta z \in \mathcal{Z}_N$. We next subtract $(7)_4$ from $(7)_5$ and test against $\mathcal{U}_M$ to obtain $(\eta_{N,M}^* + z_{N,M}^* - u^{\text{true}}, \delta v) = 0 \; \forall \delta v \in \mathcal{U}_M$. We hence obtain the simplified Euler-Lagrange equation associated with the PBDW minimization statement (5): find $(\eta_{N,M}^* \in \mathcal{U}_M, z_{N,M}^* \in \mathcal{Z}_N)$ such that

$$
\begin{aligned}
(\eta_{N,M}^*, q) + (z_{N,M}^*, q) &= (u^{\text{true}}, q) \quad \forall q \in \mathcal{U}_M \ , \\
(\eta_{N,M}^*, p) \qquad\qquad &= 0 \quad \forall p \in \mathcal{Z}_N,
\end{aligned}
\tag{8}
$$

and set $u_{N,M}^* = \eta_{N,M}^* + z_{N,M}^*$.

Note that the limited-observations saddle was derived here from the limited-observations minimization statement (5); we may instead directly obtain the limited-observations saddle (8) from the unlimited-observations saddle (4) through a simple restriction of the trial space for the first variable and the test space for the first equation to the experimentally observable space $\mathcal{U}_M \subset \mathcal{U}$ — the Galerkin recipe. We could also consider a Petrov-Galerkin approach in which $\eta_{N,M}^*$ is sought in a trial space informed by approximation requirements and different from the experimentally observable test space $\mathcal{U}_M$. Note that we may also achieve a similar effect within the Galerkin context: we retain a single trial and test space for $\eta_{N,M}^*$ and the first equation of our saddle, respectively, and instead expand $\mathcal{Z}_N$ to include approximation properties beyond the best-knowledge model.

From (8), we readily observe that $\eta_{N,M}^* \in \mathcal{U}_M \cap \mathcal{Z}_N^\perp$ and $z_{N,M}^* \in \mathcal{Z}_N$. In words, since we wish to minimize $\|\eta_{N,M}^*\|$, $\eta_{N,M}^*$ should only accommodate the part of the projection onto $\mathcal{U}_M$ which cannot be absorbed by $z_{N,M}^* \in \mathcal{Z}_N$: the part that lies in $\mathcal{Z}_N^\perp$. In particular, we note that the first equation suggests the decomposition of the observable state $\Pi_{\mathcal{U}_M} u^{\text{true}}$ into two parts: $\Pi_{\mathcal{U}_M} u^{\text{true}} = \eta_{N,M}^* + \Pi_{\mathcal{U}_M} z_{N,M}^*$. In other words, the component $z_{N,M}^*$ is chosen such that its projection onto the observable space explains the observed data for a minimal $\eta_{N,M}^*$: $\Pi_{\mathcal{U}_M} z_{N,M}^* = \Pi_{\mathcal{U}_M} u^{\text{true}} - \eta_{N,M}^*$. The size of the saddle system is $M + N$.

We finally note that we may eliminate the variable $\eta_{N,M}^*$ from the saddle (8) and write the equation solely in terms of $z_{N,M}^*$: find $z_{N,M}^* \in \mathcal{Z}_N$ such that

$$(\Pi_{\mathcal{U}_M} z_{N,M}^*, v) = (\Pi_{\mathcal{U}_M} u^{\text{true}}, v) \quad \forall v \in \mathcal{Z}_N.$$

The Galerkin statement is associated with the minimization problem: find $z_{N,M}^* \in \mathcal{Z}_N$ such that $z_{N,M}^* = \arg\inf_{z \in \mathcal{Z}_N} \|\Pi_{\mathcal{U}_M}(u^{\text{true}} - z)\|$.

2.4. Algebraic Form: Offline-Online Computational Decomposition

We consider an algebraic form of the PBDW state estimation problem (8). Towards this end, we first assume that elements of the infinite-dimensional space $\mathcal{U}$ is approximated in a suitably rich $\mathcal{N}$-dimensional approximation space $\mathcal{U}^{\mathcal{N}}$. We introduce a hierarchical basis of (the $\mathcal{N}$-dimensional representation of) $\mathcal{Z}_{N_{\max}}$: $\{\zeta_n\}_{n=1}^{N_{\max}}$ such that $\mathcal{Z}_N = \mathrm{span}\{\zeta_n\}_{n=1}^N$, $N = 1, \ldots, N_{\max}$. We similarly introduce a hierarchical basis of (the $\mathcal{N}$-dimensional representation of) $\mathcal{U}_{M_{\max}}$: $\{q_m\}_{m=1}^{M_{\max}}$ such that $\mathcal{U}_M = \mathrm{span}\{q_m\}_{m=1}^M$, $M = 1, \ldots, M_{\max}$. Any element $z \in \mathcal{Z}_N$ may be expressed as $z = \sum_{n=1}^N \zeta_n \mathbf{z}_n$ for some $\mathbf{z} \in \mathbb{R}^N$; any element $\eta \in \mathcal{U}_M$ may be expressed as $\eta = \sum_{m=1}^M q_m \boldsymbol{\eta}_m$ for some $\boldsymbol{\eta} \in \mathbb{R}^M$.

In the Offline stage, we then form matrices $\mathbf{A} \in \mathbb{R}^{M_{\max} \times M_{\max}}$ and $\mathbf{B} \in \mathbb{R}^{M_{\max} \times N_{\max}}$ such that

$$\mathbf{A}_{mm'} = (q_{m'}, q_m), \quad m, m' = 1, \ldots, M_{\max},$$
$$\mathbf{B}_{mn} = (\zeta_n, q_m), \quad m = 1, \ldots, M_{\max}, \ n = 1, \ldots, N_{\max}.$$

If we wish to evaluate a functional output $\ell^{\mathrm{out}}(u^*_{N,M})$, then we in addition form vectors $\mathbf{l}^{\mathrm{out},U} \in \mathbb{R}^{M_{\max}}$ and $\mathbf{l}^{\mathrm{out},Z} \in \mathbb{R}^{N_{\max}}$ such that

$$(\mathbf{l}^{\mathrm{out},U})_m = \ell^{\mathrm{out}}(q_m), \quad m = 1, \ldots, M_{\max},$$
$$(\mathbf{l}^{\mathrm{out},Z})_n = \ell^{\mathrm{out}}(\zeta_n), \quad n = 1, \ldots, N_{\max}.$$

The computation of the elements of $\mathcal{Z}_{N_{\max}}$ and $\mathcal{U}_{M_{\max}}$ and the formation of the matrices and vectors require $\mathcal{O}(\mathcal{N}^\cdot)$ operations for some exponent that depends on the particular $\mathcal{Z}_N$ and $\mathcal{U}_M$ generation strategies.

In the Online stage, we solve the algebraic form of (8): find $\boldsymbol{\eta}^* \in \mathbb{R}^M$ and $\mathbf{z}^* \in \mathbb{R}^N$ such that

$$\begin{pmatrix} \mathbf{A}_{1:M,1:M} & \mathbf{B}_{1:M,1:N} \\ \mathbf{B}^H_{1:M,1:N} & 0 \end{pmatrix} \begin{pmatrix} \boldsymbol{\eta}^* \\ \mathbf{z}^* \end{pmatrix} = \begin{pmatrix} l^{\mathrm{obs}}_M \\ 0 \end{pmatrix};$$

here $\mathbf{A}_{1:M,1:M} \in \mathbb{R}^{M \times M}$ denotes the $M \times M$ principal submatrix of $\mathbf{A}$, $\mathbf{B}_{1:M,1:N} \in \mathbb{R}^{M \times N}$ denotes the $M \times N$ principal submatrix of $\mathbf{B}$, $(\cdot)^T$ denotes the transpose, and $\mathbf{l}^{\mathrm{obs}} \in \mathbb{R}^M$ is the M-vector of experimentally observed values, $\mathbf{l}^{\mathrm{obs}}_m = \ell^{\mathrm{o}}(u^{\mathrm{true}})$, $m = 1, \ldots, M$. The solution of the saddle system requires $\mathcal{O}((N + M)^3)$ operations.

Once the coefficients $\boldsymbol{\eta}^* \in \mathbb{R}^M$ and $\mathbf{z}^* \in \mathbb{R}^N$ are computed, we may find the field $u^*_{N,M}$ and the output $\ell^{\mathrm{out}}(u^*_{N,M})$. Specifically, the state is given by $u^*_{N,M} = \eta^*_{N,M} + z^*_{N,M} = \sum_{m=1}^M q_m \boldsymbol{\eta}^*_m + \sum_{n=1}^N \zeta_n \mathbf{z}^*_n$; the evaluation requires $\mathcal{O}(\mathcal{N})$ operations. The output is given by $\ell^{\mathrm{out}}(u^*_{N,M}) = \sum_{m=1}^M \mathbf{l}^{\mathrm{out},U}_m \boldsymbol{\eta}^*_m + \sum_{n=1}^N \mathbf{l}^{\mathrm{out},Z}_n \mathbf{z}^*_n$; the evaluation requires $\mathcal{O}(N + M)$ operations.

2.5. A Priori Error Analysis

2.5.1. Field Estimates.
We appeal to the variational construction of the PBDW estimate and the existent theory on finite element analysis (see, for example, [24]) to develop an *a priori* error theory for the PBDW formulation. We first state a proposition on the state (field) estimation error.

Proposition 2. The PBDW approximation error satisfies

$$\|\eta^*_N - \eta^*_{N,M}\| \le \inf_{q \in \mathcal{U}_M \cap \mathcal{Z}_N^\perp} \inf_{z \in \mathcal{Z}_N} \|u^{\mathrm{true}} - z - q\|,$$

$$\|z^*_N - z^*_{N,M}\| \le \frac{1}{\beta_{N,M}} \inf_{q \in \mathcal{U}_M \cap \mathcal{Z}_N^\perp} \inf_{z \in \mathcal{Z}_N} \|u^{\mathrm{true}} - z - q\|,$$

$$\|u^{\mathrm{true}} - u^*_{N,M}\| \le \left(1 + \frac{1}{\beta_{N,M}}\right) \inf_{q \in \mathcal{U}_M \cap \mathcal{Z}_N^\perp} \inf_{z \in \mathcal{Z}_N} \|u^{\mathrm{true}} - z - q\|,$$

where the stability constant $\beta_{N,M}$ is defined by

$$\beta_{N,M} \equiv \inf_{z \in \mathcal{Z}_N} \sup_{q \in \mathcal{U}_M} \frac{(z,q)}{\|z\|\|q\|}.$$

Proof

We subtract $(8)_1$ from $(4)_1$ and test against $q \in \mathcal{U}_M \cap \mathcal{Z}_N^\perp$ to obtain

$$(\eta_N^* - \eta_{N,M}^*, q) = 0 \quad \forall q \in \mathcal{U}_M \cap \mathcal{Z}_N^\perp.$$

It follows that, for any $q \in \mathcal{U}_M \cap \mathcal{Z}_N^\perp$,

$$\|\eta_N^* - \eta_{N,M}^*\|^2 = (\eta_N^* - \eta_{N,M}^*, \eta_N^* - q) + (\eta_N^* - \eta_{N,M}^*, q - \eta_{N,M}^*) \leq \|\eta_N^* - \eta_{N,M}^*\|\|\eta_N^* - q\|;$$

note that, in the last step, the second term vanishes: $(\eta_N^* - \eta_{N,M}^*, q - \eta_{N,M}^*) = 0$ since $q - \eta_{N,M}^* \in \mathcal{U}_M \cap \mathcal{Z}_N^\perp$. We thus obtain

$$\|\eta_N^* - \eta_{N,M}^*\| \leq \inf_{q \in \mathcal{U}_M \cap \mathcal{Z}_N^\perp} \|\eta_N^* - q\|.$$

Since $\eta_N^* = \Pi_{\mathcal{Z}_N^\perp} u^{\text{true}}$ and $q \in \mathcal{Z}_N^\perp$,

$$\begin{aligned}
\|\eta_N^* - \eta_{N,M}^*\|^2 &\leq \inf_{q \in \mathcal{U}_M \cap \mathcal{Z}_N^\perp} \|\Pi_{\mathcal{Z}_N^\perp} u^{\text{true}} - q\|^2 \\
&= \inf_{z \in \mathcal{Z}_N} \|\Pi_{\mathcal{Z}_N} u^{\text{true}} - z\|^2 + \inf_{q \in \mathcal{U}_M \cap \mathcal{Z}_N^\perp} \|\Pi_{\mathcal{Z}_N^\perp} u^{\text{true}} - q\|^2 \\
&= \inf_{q \in \mathcal{U}_M \cap \mathcal{Z}_N^\perp} \inf_{z \in \mathcal{Z}_N} \left(\|\Pi_{\mathcal{Z}_N} u^{\text{true}} - z\|^2 + \|\Pi_{\mathcal{Z}_N^\perp} u^{\text{true}} - q\|^2 \right) \\
&= \inf_{q \in \mathcal{U}_M \cap \mathcal{Z}_N^\perp} \inf_{z \in \mathcal{Z}_N} \|\Pi_{\mathcal{Z}_N} u^{\text{true}} - z + \Pi_{\mathcal{Z}_N^\perp} u^{\text{true}} - q\|^2 \\
&= \inf_{q \in \mathcal{U}_M \cap \mathcal{Z}_N^\perp} \inf_{z \in \mathcal{Z}_N} \|u^{\text{true}} - z - q\|^2.
\end{aligned}$$

Here, the first equality follows since $\inf_{z \in \mathcal{Z}_N} \|\Pi_{\mathcal{Z}_N} u^{\text{true}} - z\|^2 = 0$; the third equality follows from the Pythagorean theorem since $\Pi_{\mathcal{Z}_N} u^{\text{true}} - z \in \mathcal{Z}_N$ and $\Pi_{\mathcal{Z}_N^\perp} u^{\text{true}} - q \in \mathcal{Z}_N^\perp$. It follows that

$$\|\eta_N^* - \eta_{N,M}^*\| \leq \inf_{q \in \mathcal{U}_M \cap \mathcal{Z}_N^\perp} \inf_{z \in \mathcal{Z}_N} \|u^{\text{true}} - z - q\|, \tag{9}$$

which is the bound on $\|\eta_N^* - \eta_{N,M}^*\|$.

We next subtract $(8)_1$ from $(4)_1$ and test against $q \in \mathcal{U}_M$ to obtain

$$(\eta_N^* - \eta_{N,M}^*, q) + (z_N^* - z_{N,M}^*, q) = 0 \quad \forall q \in \mathcal{U}_M.$$

It follows from $z_N^* - z_{N,M}^* \in \mathcal{Z}_N$ and the definition of the inf-sup constant that

$$\beta_{N,M} \|z_N^* - z_{N,M}^*\| \leq \sup_{v \in \mathcal{U}_M} \frac{(z_N^* - z_{N,M}^*, v)}{\|v\|} = \sup_{v \in \mathcal{U}_M} \frac{-(\eta_N^* - \eta_{N,M}^*, v)}{\|v\|} \leq \|\eta_N^* - \eta_{N,M}^*\|.$$

Combined with (9), we obtain

$$\|z_N^* - z_{N,M}^*\| \leq \frac{1}{\beta_{N,M}} \inf_{q \in \mathcal{U}_M \cap \mathcal{Z}_N^\perp} \inf_{z \in \mathcal{Z}_N} \|u^{\text{true}} - z - q\|,$$

which is the bound on $\|z_N^* - z_{N,M}^*\|$.

We finally invoke the triangle inequality,

$$\|u^{\text{true}} - u_{N,M}^*\| \leq \|\eta_N^* - \eta_{N,M}^*\| + \|z_N^* - z_{N,M}^*\| \leq \left(1 + \frac{1}{\beta_{N,M}}\right) \inf_{q \in \mathcal{U}_M \cap \mathcal{Z}_N^\perp} \inf_{z \in \mathcal{Z}_N} \|u^{\text{true}} - z - q\|,$$

which is the bound on $\|u^{\text{true}} - u_{N,M}^*\|$. $\qquad\square$

Proposition 2 identifies three distinct contributions to the error in the field estimate. First is the stability constant, $\beta_{N,M}$; better the stability, smaller the error. Second is the background best-fit error, $\inf_{z \in \mathcal{Z}_N} \|u^{\text{true}} - z\|$; the error is small if u^{true} is well approximated in the background space $\mathcal{Z}_N$. Third is the update best-fit error, $\inf_{q \in \mathcal{U}_M \cap \mathcal{Z}_N^\perp} \|\Pi_{\mathcal{Z}_N^\perp} u^{\text{true}} - q\|$; the components of u^{true} that do not lie in $\mathcal{Z}_N$ is treated by the update space. We will appeal in Section 2.7 to these observations to select $\mathcal{Z}_N$ and $\mathcal{U}_M$.

2.5.2. Output Estimates. We may also develop an *a priori* error bound associated with an estimate of a functional output.

Proposition 3. Let $\ell^{\text{out}} \in \mathcal{U}'$ be the output functional of interest. The output error satifies

$$|\ell^{\text{out}}(u^{\text{true}}) - \ell^{\text{out}}(u^*_{N,M})| = |(u^{\text{true}} - u^*_{N,M}, \psi - \Pi_{\mathcal{U}_M}\psi)|$$
$$\leq \|u^{\text{true}} - u^*_{N,M}\|\|\psi - \Pi_{\mathcal{U}_M}\psi\|$$

for the adjoint $\psi = R_\mathcal{U} \ell^{\text{out}} \in \mathcal{U}$.

Proof
We first note that

$$\ell^{\text{out}}(w) = (R_\mathcal{U} \ell^{\text{out}}, w) = (\psi, w) \quad \forall w \in \mathcal{U}$$

by the definition of the Riesz operator and the adjoint ψ. We next note that, by Galerkin orthogonality, $(u^{\text{true}} - u^*_{N,M}, q) = 0 \ \forall q \in \mathcal{U}_M$. It follows that

$$|\ell^{\text{out}}(u^{\text{true}} - u^*_{N,M})| = |(u^{\text{true}} - u^*_{N,M}, \psi)| = |(u^{\text{true}} - u^*_{N,M}, \psi - \Pi_{\mathcal{U}_M}\psi)|.$$

We finally invoke Cauchy-Schwarz to obtain the desired bound. $\square$

Proposition 3 suggests that the error in a functional output depends on, in addition to the factors that affect the field estimate, the approximation of the adjoint by the update space. Similar to the finite element approximation, we expect the output estimate to "superconverge" with M, as both the approximation of the primal and adjoint states contributes to the reduction in the output error.

2.5.3. Stabilization. Proposition 2 shows that the stability constant $\beta_{N,M}$ plays a key role in controlling the state estimation error. As regard its behavior, we have the following proposition.

Proposition 4. The inf-sup constant

$$\beta_{N,M} \equiv \inf_{z \in \mathcal{Z}_N} \sup_{q \in \mathcal{U}_M} \frac{(z,q)}{\|z\|\|q\|}$$

is a non-increasing function of background span (N) and a non-decreasing function of observable span (M). Furthermore, $\beta_{N,M} = 0$ for $M < N$.

Proof
The result is a direct consequence of the expansion of the infimizer space $\mathcal{Z}_N$ and the supremizer space $\mathcal{U}_M$. $\square$

2.5.4. Approximation Properties of $\mathcal{U}_M$ for Pointwise Measurements in One Dimension.
Proposition 2 suggests that the update space $\mathcal{U}_M$ plays a role in estimating the component of
state that lies in $\mathcal{Z}_N^\perp$. We hence wish to quantify the approximation properties of the space
$\mathcal{U}_M$. We do not have a characterization of the approximation properties for a general physical
dimension d, inner product $(\cdot, \cdot)$, and output functional $\ell_m^o(\cdot)$; we can however quantify the
approximation properties in a very specialized case.

Proposition 5. Let $\Omega \subset]0, 1[$, $\|\cdot\| = |\cdot|_{H^1(\Omega)}$, and $u^{\text{true}} \in H_0^1(\Omega) \cap H^2(\Omega)$. Consider
pointwise observation functionals $\ell_m^o \equiv \delta(\cdot, x_m^o)$, $m = 1, \ldots, M$, with uniformly spaced centers
$\{x_m^o\}_{m=1}^M$. We denote the associated update space by $\mathcal{U}_M \equiv \text{span}\{R_\mathcal{U}\ell_m^o\}_{m=1}^M$. Then, the update
best-fit error is bounded by

$$\inf_{q \in \mathcal{U}_M} \|u^{\text{true}} - q\|_{H^r(\Omega)} \leq CM^{-(2-r)}\|u^{\text{true}}\|_{H^2(\Omega)}$$

for $r = 0, 1$ and some C independent of M and u^{true}.

Proof
Since $u^{\text{true}} \in H_0^1(\Omega) \cap H^2(\Omega)$ and $\|\cdot\| = |\cdot|_{H^1(\Omega)}$, it suffices to show that $\mathcal{U}_M$ is a space of
piecewise linear polynomials,

$$\mathcal{X}_M \equiv \{w \in C^0(\Omega) \mid w|_{I_k} \in \mathbb{P}^1(I_k), k = 1, \ldots, M+1\},$$

for $I_1 = [0, x_1]$, $I_{M+1} = [x_M, 1]$, and $I_k = [x_k, x_{k+1}]$, $k = 2, \ldots, M-1$. (Without loss of
generality, we assume $0 \leq x_1 < \cdots < x_M \leq 1$.) Towards this end, we first note that for
$\ell_m^o = \delta(\cdot, x_m^o)$ and $\|\cdot\| = |\cdot|_{H^1(\Omega)}$, a function $R_\mathcal{U}\ell_m^o \in \mathcal{U}$ is the piecewise linear "hat" function
with the peak (or the derivative jump) at x_m^o; in particular $R_\mathcal{U}\ell_m^o \in \mathcal{U}_M$. We then note that
the functions $\{R_\mathcal{U}\ell_m^o\}_{m=1}^M$ are linearity independent because x_m^o (and hence the location
of the derivative jumps) are different. We thus have M linearly independent functions
in the M-dimensional space $\mathcal{U}_M$; thus, $\{R_\mathcal{U}\ell_m^o\}_{m=1}^M$ is a basis for $\mathcal{U}_M$ and in particular
$\mathcal{U}_M \equiv \text{span}\{R_\mathcal{U}\ell_m^o\}_{m=1}^M = \mathcal{X}_M$. This concludes the proof. $\qquad\square$

On one hand, Proposition 5 shows that we can expect the update best-fit error error to
decrease with M and hence, combined with Proposition 2, $u_{N,M}^*$ converges to u^{true} in the limit
of $M \to \infty$. On the other hand, Proposition 5 shows that the convergence of the error with the
number of observations M is rather slow: the $H^1(\Omega)$ and $L^2(\Omega)$ error converges as M^{-1} and
M^{-2}, respectively, in one dimension. More generally, we expect the $H^1(\Omega)$ and $L^2(\Omega)$ error
to converge as $M^{-1/d}$ and $M^{-2/d}$, respectively, in a d-dimensional space. In order to obtain a
good estimate with a reasonable number of observations M, we must choose the background
space $\mathcal{Z}_N$ appropriately such that the update $\eta_N^* \in \Pi_{\mathcal{Z}_N^\perp}u^{\text{true}}$ is small.

2.6. A Posteriori Error Estimates

We introduce an *a posteriori* error estimate for the state estimate $u_{N,M}^*$,

$$E_{N,M,M'} \equiv \|u_{N,M'}^* - u_{N,M}^*\|,$$

where M', such that $M \leq M' \leq M_{\max}$, is the number of observations used to form the
error estimate. We similarly introduce an *a posteriori* error estimate for the output estimate
$\ell^{\text{out}}(u_{N,M}^*)$,

$$O_{N,M,M'} \equiv |\ell^{\text{out}}(u_{N,M'}^*) - \ell^{\text{out}}(u_{N,M}^*)|,$$

again based on $M' \geq M$ observations. We note that, for $M' = M$, $E_{N,M,M'} = 0$ and $O_{N,M,M'} = 0$.

Remark 1. The field *a posteriori* error estimate $E_{N,M,M'}$ may be interpreted as an approximation of the (dual) norm of the error $u^{\mathrm{true}} - u^*_{N,M}$ using the M'-dimensional subspace $\mathcal{U}'_M \subset \mathcal{U}$ as the test space:

$$E_{N,M,M'} = \sup_{q \in \mathcal{U}_{M'}} \frac{|(u^{\mathrm{true}}, q) - (u^*_{N,M}, q)|}{\|q\|}.$$

The equivalence follows from $(u^*_{N,M'}, q) = (u^{\mathrm{true}}, q)\ \forall q \in \mathcal{U}_{M'}$. Assuming $\mathcal{U}_{M'} \to \mathcal{U}$ as $M' \to \infty$, the (dual) norm estimate converges to the true (dual) norm of the error.

2.7. Construction of Spaces: Offline

2.7.1. Best-Knowledge Model. As we have just described, Proposition 2 suggests that we should choose the background space $\mathcal{Z}_N$ such that the background best-fit error $\inf_{z \in \mathcal{Z}_N} \|u^{\mathrm{true}} - z\|$ is small. We consider a parametric construction of the spaces $\mathcal{Z}_N$, $N = 1, \ldots, N_{\max}$, such that the background best-fit error decreases rapidly with N.

Towards this end, we now formally introduce the parametrized best-knowledge model previously discussed in the introduction. We first introduce a parameter $\mu \in \mathcal{D}$; here, $\mathcal{D} \subset \mathbb{R}^P$ is the parameter domain associated with the anticipated, or parametric, uncertainty in the best-knowledge model. We next introduce a parametrized form: $G^\mu : \mathcal{U} \times \mathcal{U} \to \mathbb{R}$; we assume that the form is linear in the second argument. We then define, for a given $\mu \in \mathcal{D}$, the best-knowledge solution $u^{\mathrm{bk},\mu} \in \mathcal{U}$ that satisfies

$$G^\mu(u^{\mathrm{bk},\mu}, v) = 0 \quad \forall v \in \mathcal{U};$$

we assume that the problem is well posed; that is, for any $\mu \in \mathcal{D}$, $u^{\mathrm{bk},\mu}$ exists and is unique. We now introduce the best-knowledge parametrized manifold

$$\mathcal{M}^{\mathrm{bk}} \equiv \{u^{\mathrm{bk},\mu} \mid \mu \in \mathcal{D}\}.$$

We intend to choose the parametrized form G^μ and the parameter domain $\mathcal{D}$ to minimize the model error

$$\epsilon^{\mathrm{bk}}_{\mathrm{mod}}(u^{\mathrm{true}}) \equiv \inf_{w \in \mathcal{M}^{\mathrm{bk}}} \|u^{\mathrm{true}} - w\| = \|u^{\mathrm{true}} - F_{\mathcal{M}^{\mathrm{bk}}} u^{\mathrm{true}}\|,$$

where $F_{\mathcal{M}^{\mathrm{bk}}} u^{\mathrm{true}} \in \mathcal{M}^{\mathrm{bk}}$ is the infimizer.

2.7.2. Background Spaces $\mathcal{Z}_N$. As mentioned in the introduction, we condense the best-knowledge of $\mathcal{M}^{\mathrm{bk}}$ into a N-dimensional linear space $\mathcal{Z}_N$ through several different model reduction processes: $\mathrm{PROCESS}^{\mathcal{Z}}_N(\mathcal{M}^{\mathrm{bk}}) \to \mathcal{Z}_N$. Here we list a few:

- Proper orthogonal decomposition (POD): $\mathrm{PROCESS}^{\mathcal{Z}}_N(\mathcal{M}^{\mathrm{bk}}) \equiv \mathrm{POD}_N(\mathcal{M}^{\mathrm{bk}})$.
  We first introduce a training set $\Xi_{\mathrm{train}} \subset \mathcal{D}$ that sufficiently covers the parameter domain $\mathcal{D}$. We then evaluate the best-knowledge solution at each training point to form the set $\{u^{\mathrm{bk},\mu}\}_{\mu \in \Xi_{\mathrm{train}}}$. We finally apply POD [14] to $\{u^{\mathrm{bk},\mu}\}_{\mu \in \Xi_{\mathrm{train}}}$ and extract the N most dominant modes as measured in $\| \cdot \|$ to form $\mathcal{Z}_N$.
- Weak Greedy: $\mathrm{PROCESS}^{\mathcal{Z}}_N(\mathcal{M}^{\mathrm{bk}}) \equiv \mathrm{WEAKGREEDY}_N(\mathcal{M}^{\mathrm{bk}})$.
  We apply the Weak Greedy algorithm described in Algorithm 1 to form $\mathcal{Z}_N$ (see also a detailed review — in particular as regard the construction of an error bound that is efficient in the many-query setting — by Rozza *et al.* [25]). The algorithm has been proven to generate an optimal sequence of spaces with respect to the Kolmogorov width of $\mathcal{M}^{\mathrm{bk}}$ in Binev *et al.* [3], Buffa *et al.* [4], and DeVore *et al.* [7].
- Taylor expansion: $\mathrm{PROCESS}^{\mathcal{Z}}_N(\mathcal{M}^{\mathrm{bk}}) \equiv \mathrm{TAYLOR}^{\mu_0}_N(\mathcal{M}^{\mathrm{bk}})$.
  We first evaluate the parametric derivatives of the solution $u^{\mathrm{bk},\mu}$: $\zeta_p \in \mathcal{U}$ such that $\frac{\partial}{\partial \mu_p} G^\mu(\zeta_p, v)|_{\mu = \mu_0}\ \forall v \in \mathcal{U}$, $p = 1, \ldots, P$. We then form $\mathcal{Z}_{N=P} = \mathrm{span}\{\zeta_p\}^P_{p=1}$. We may also consider higher-order expansions [9].

Algorithm 1: WeakGreedy$_M$ Algorithm

---

   input : G^μ: parametrized best-knowledge model

           $\mathcal{D}$: parameter domain

           $\Delta_N^{\mathrm{bk},\mu}$: error estimate for $\inf_{z \in \mathcal{Z}_N} \|u^{\mathrm{bk},\mu} - z\| \leq \Delta_N^{\mathrm{bk},\mu}$

   output: $\{\mathcal{Z}_N\}_{N=1}^{N_{\max}}$: N-dimensional hierarchical background space

---

1 for $M = 1, \ldots, N_{\max}$ **do**

2   Identify the parameter associated with the largest error estimate

$$\tilde{\mu}_N = \underset{\mu \in \Xi_{\mathrm{train}} \in \mathcal{D}}{\arg\sup} \Delta_{N-1}^{\mathrm{bk},\mu}$$

3   Evaluate the associated solution

$$\zeta_N = u_{\tilde{\mu}_N}^{\mathrm{bk}}$$

4   Augment the background space

$$\mathcal{Z}_N = \mathrm{span}\{\mathcal{Z}_{N-1}, \zeta_N\}$$

5 end

- Superposition: $\textsc{Process}_N^{\mathcal{Z}}(\mathcal{M}^{\mathrm{bk}}) \equiv \textsc{Superposition}_N(\mathcal{M}^{\mathrm{bk}})$.

  We consider a hierarchical set of N functions that 1) solves the homogeneous PDE and 2) provides rapidly converging approximation with N. These functions are effectively parametrized by an appropriate truncated representation of the trace on $\partial\Omega$. For instance, in the context of Helmholtz equations, we may consider the Fourier-Bessel functions [5]. (Conceptually, the method is a special case of $\textsc{WeakGreedy}_N$ applied to a best-knowledge model with parametrized boundary conditions; computationally, we may take advantage of the closed form expressions for the homogeneous solutions.)

We may also consider other model order reduction approaches, such as the Proper Generalized Decomposition (PGD) [15].

In general, we may quantify the approximation property of the background space in terms of the best-fit error

$$\epsilon_N^{\mathrm{bk}}(u^{\mathrm{true}}) \equiv \inf_{w \in \mathcal{Z}_N} \|u^{\mathrm{true}} - w\|.$$

In particular, if the space $\mathcal{Z}_N$ is generated from the best-knowledge manifold $\mathcal{M}^{\mathrm{bk}}$, we may decompose the error into two parts and identify two different sources of the error:

$$\begin{aligned}
\epsilon_N^{\mathrm{bk}}(u^{\mathrm{true}}) \equiv \inf_{w \in \mathcal{Z}_N} \|u^{\mathrm{true}} - w\| &\leq \|u^{\mathrm{true}} - \Pi_{\mathcal{Z}_N} F_{\mathcal{M}^{\mathrm{bk}}}(u^{\mathrm{true}})\| \\
&\leq \|u^{\mathrm{true}} - F_{\mathcal{M}^{\mathrm{bk}}}(u^{\mathrm{true}})\| + \|F_{\mathcal{M}^{\mathrm{bk}}}(u^{\mathrm{true}}) - \Pi_{\mathcal{Z}_N} F_{\mathcal{M}^{\mathrm{bk}}}(u^{\mathrm{true}})\| \\
&\leq \inf_{w \in \mathcal{M}^{\mathrm{bk}}} \|u^{\mathrm{true}} - w\| + \sup_{w \in \mathcal{M}^{\mathrm{bk}}} \|w - \Pi_{\mathcal{Z}_N} w\| \\
&\leq \epsilon_{\mathrm{mod}}^{\mathrm{bk}}(u^{\mathrm{true}}) + \epsilon_{\mathrm{disc},N}^{\mathrm{bk}}.
\end{aligned}$$

The first term, $\epsilon_{\mathrm{mod}}^{\mathrm{bk}}(u^{\mathrm{true}}) \equiv \inf_{w \in \mathcal{M}^{\mathrm{bk}}} \|u^{\mathrm{true}} - w\|$, is the *modeling error*, which arise from the fact that we cannot in general anticipate all forms of uncertainty and provide the associated parametrized model; hence, in general, $u^{\mathrm{true}} \notin \mathcal{M}^{\mathrm{bk}}$, and $\epsilon_{\mathrm{mod}}^{\mathrm{bk}}(u^{\mathrm{true}}) \neq 0$. The second term, $\epsilon_{\mathrm{disc},N}^{\mathrm{bk}} \equiv \sup_{w \in \mathcal{M}^{\mathrm{bk}}} \|w - \Pi_{\mathcal{Z}_N} w\|$, is the *discretization error*, which arise from the fact we cannot in general construct a N-dimensional linear space that can represent all elements

of $\mathcal{M}^{\mathrm{bk}}$; hence, in general, $\mathcal{M}^{\mathrm{bk}} \not\subset \mathcal{Z}_N$, and $\epsilon_{\mathrm{disc},N}^{\mathrm{bk}} \neq 0$. For some constructions of $\mathcal{Z}_N$, we may rigorously bound the *discretization* error; for example, in the Weak Greedy procedure, $\epsilon_{\mathrm{disc},N}^{\mathrm{bk}} = \Delta_N^{\mathrm{bk},\mu}$. On the other hand, we cannot in general bound the *modeling* error.

2.7.3. Superdomains for the Best-Knowledge Model. As mentioned in the introduction, projection-by-data, unlike projection-by-model, does not require boundary conditions (and initial conditions). However, in order to obtain best-knowledge solutions and to construct $\mathcal{Z}_N$, the best-knowledge model must be defined on a domain on which the boundary-value problem is well posed. Hence, in general, the domain on which we wish to estimate the state, $\Omega \subset \mathbb{R}^d$, may differ from the domain associated with the best-knowledge model, $\Omega^{\mathrm{bk}} \supset \Omega$. More generally, the domain Ω may be a manifold in Ω^{bk}: $\Omega^{\mathrm{bk}} \subset \mathbb{R}^{d'}$ for $d' > d$.

In this generalized setting, to construct $\mathcal{Z}_N$, we first identify the Hilbert space associated with Ω^{bk} by $\mathcal{U}^{\mathrm{bk}} = \mathcal{U}^{\mathrm{bk}}(\Omega^{\mathrm{bk}})$. We then identify the best-knowledge manifold, $\mathcal{M}^{\mathrm{bk}} \equiv \{u^{\mathrm{bk},\mu} \in \mathcal{U}^{\mathrm{bk}} \mid \mu \in \mathcal{D}\}$. We next construct the background space on Ω^{bk}, $\mathrm{PROCESS}_N^{\mathcal{Z}}(\mathcal{M}^{\mathrm{bk}}) \to \mathcal{Z}_N^{\mathrm{bk}}$. We finally form the background space on Ω, $\mathcal{Z}_N = \{z \in \mathcal{U} \mid z = z^{\mathrm{bk}}|_\Omega, \ z^{\mathrm{bk}} \in \mathcal{Z}^{\mathrm{bk}}\}$. The procedure allows us to focus on data assimilation on $\Omega \subset \Omega^{\mathrm{bk}}$ even if the best-knowledge model is only well posed on $\Omega^{\mathrm{bk}} \supset \Omega$.

2.7.4. Experimentally Observable Update Spaces $\mathcal{U}_M$: Design of Experiment. Proposition 2 shows that, for a given $\mathcal{Z}_N$, the selection of the experimentally observable update spaces $\mathcal{U}_M$ should be based on two criteria:

- the maximization of the stability constant $\beta_{N,M} = \inf_{w \in \mathcal{Z}_N} \sup_{v \in \mathcal{U}_M} (w,v)/(\|w\|\|v\|)$; to improve stability, we wish to choose $\mathcal{U}_M$ such that any element in $\mathcal{Z}_N$ is well approximated by an element in $\mathcal{U}_M$.
- the minimization of the approximation error $\inf_{\eta \in \mathcal{U}_M \cap \mathcal{Z}_N^\perp} \|\Pi_{\mathcal{Z}_N^\perp} u^{\mathrm{true}} - \eta\|$; to improve approximation, we wish to choose $\mathcal{U}_M$ such that elements in $\mathcal{Z}_N^\perp$ — that is elements outside of $\mathcal{Z}_N$ — are well approximated by $\mathcal{U}_M$.

We emphasize that $\mathcal{U}_M$ must be experimentally observable: $\mathcal{U}_M = \mathrm{span}\{q_m \equiv R_{\mathcal{U}} \ell_m^{\mathrm{o}}\}_{m=1}^M$, $M = 1, \ldots, M_{\mathrm{max}}$. Note that, by construction, the experimentally observable space is a function of the choice of the inner product $(\cdot, \cdot)$.

We recall that, even though the PBDW framework may accommodate any observation functional that is consistent with the data-acquisition procedure, in this paper we focus on localized observations. As noted, for localized observations using a given transducer, $\ell_m^{\mathrm{o}}(\cdot) = \mathrm{Gauss}(\cdot; x_m^{\mathrm{c}}, r_m)$, the location of the centers $\{x_m^{\mathrm{c}}\}_{m=1}^M$ largely determine the space $\mathcal{U}_M$. We may select the observation functionals (and more specifically the observation centers) using several different processes: $\mathrm{PROCESS}_M^{\mathcal{U}}(\mathcal{Z}_{N_{\mathrm{max}}}) \to \mathcal{U}_M$. Here we list a few:

- Quasi-uniform or random: $\mathrm{PROCESS}_M^{\mathcal{U}}(\mathcal{Z}_{N_{\mathrm{max}}}) \equiv \mathrm{QUASIUNIFORM}_M$ or $\mathrm{RANDOMUNIFORM}_M$. The algorithm aims to minimize the approximation error by providing a uniform coverage of the domain. $\mathrm{QUASIUNIFORM}_M$ is a deterministic sequential procedure: at step m, we insert a new point at the location which maximizes the shortest distance to the set of points at step $m - 1$. $\mathrm{RANDOMUNIFORM}_M$ is a stochastic sequential procedure: we simply draw points sequentially from the uniform density over Ω.
- Generalized Empirical Interpolation Method [18]: $\mathrm{PROCESS}_M^{\mathcal{U}}(\mathcal{Z}_{N_{\mathrm{max}}}) \equiv \mathrm{GEIM}_M(\mathcal{Z}_{N_{\mathrm{max}}})$. In particular, we employ the point selection routine designed to minimize the Lebesgue constant associated with the approximation space $\mathcal{Z}_{N_{\mathrm{max}}} \subset \mathcal{U}$ in a greedy manner. The algorithm works for $M = N$, $N = 1, \ldots, N_{\mathrm{max}}$.
- Greedy stability maximization: $\mathrm{PROCESS}_M^{\mathcal{U}}(\mathcal{Z}_{N_{\mathrm{max}}}) \equiv \mathrm{SGREEDY}_M(\mathcal{Z}_{N_{\mathrm{max}}})$. The procedure is described in Algorithm 2. In short, the algorithm maximizes the inf-sup constant $\beta_{N,M}$ in a greedy manner. Unlike the GEIM_M algorithm above, the $\mathrm{SGREEDY}_M$ algorithm is applicable for $M > N$. The $\mathrm{SGREEDY}_M$ algorithm is equivalent to GEIM_M for $M = N$.

Algorithm 2: SGREEDY$_M$ Stability-Maximization Algorithm

---

   input : $\{\mathcal{Z}_N\}_{N=1}^{N_{\max}}$: background approximation spaces

   output: $\{\mathcal{U}_M\}_{M=1}^{M_{\max}}$: experimentally observable update spaces

1 **for** $M = 1, \ldots, M_{\max}$ **do**

2   Set $N = \min\{N_{\max}, M\}$.

3   Compute the least-stable mode: for $M > 1$,

$$w_{\inf} = \arg\inf_{w \in \mathcal{Z}_N} \sup_{v \in \mathcal{U}_{M-1}} \frac{(w, v)}{\|w\|\|v\|};$$

        for $M = 1$, set $w_{\inf}$ to a normalized basis for $\mathcal{Z}_{N=M=1}$.

4   Compute the associated supremizer

$$v_{\sup} = \Pi_{\mathcal{U}_{M-1}} w_{\inf}.$$

5   Identify the least well-approximated point

$$\tilde{x} = \arg\sup_{x \in \Omega} |(w_{\inf} - v_{\sup})(x)|.$$

6   Set

$$\mathcal{U}_M = \text{span}\{\mathcal{U}_{M-1}, R_{\mathcal{U}}\text{Gauss}(\cdot; \tilde{x}, r_M)\}.$$

7 **end**

- Greedy stability-approximation balancing [26]: PROCESS$_M^{\mathcal{U}}(\mathcal{Z}_{N_{\max}}) \equiv$ SAGREEDY$(\mathcal{Z}_{N_{\max}})$. The algorithm is a combination of the above SGREEDY$_M$ and RANDOMUNIFORM$_M$ algorithms. We initially invoke the SGREEDY algorithm to maximize the stability until a user-specified threshold stability constant is achieved for $N = N_{\max}$. We then invoke RANDOMUNIFORM$_M$ sampling to minimize the approximation error. Note that, because the stability constant is a non-decreasing function of M for a fixed N, the stability constant remains above the threshold in the second stage.

We will see in the results section that the stability-maximization algorithm provide more stable estimate of the state than a set of random points especially when M is close to N.

3. SYNTHETIC PROBLEM: HELMHOLTZ IN $\mathbb{R}^2$

3.1. Model Form

We study the behavior of the PBDW formulation using a two-dimensional Helmholtz problem. Towards this end, we consider a complex extension of the PBDW formulation presented in Section 2. We first introduce a domain $\Omega \equiv]0, 1[^2$ and the Hilbert space $\mathcal{U} \equiv H^1(\Omega)$ endowed with the standard H^1 inner product and norm:

$$(w, v) \equiv \int_\Omega (\nabla w \cdot \nabla \bar{v} + w\bar{v}) dx \quad \text{and} \quad \|w\| \equiv \sqrt{(w, w)}.$$

We then consider the following weak statement: find $\Upsilon_g^\mu \in \mathcal{U}$ such that

$$a^\mu(\Upsilon_g^\mu, v) = f_g^\mu(v) \quad \forall v \in \mathcal{U},$$

where

$$a^\mu(w, v) \equiv (1 + i\epsilon\mu) \int_\Omega \nabla w \cdot \nabla \bar{v} dx - \mu^2 \int_\Omega w\bar{v} dx \quad \forall w, v \in \mathcal{U},$$

$$f_g^\mu(v) \equiv \mu \int_\Omega (2x_1^2 + \exp(x_2))\bar{v} dx + \mu \int_\Omega g\bar{v} dx \quad \forall v \in \mathcal{U},$$

for a parameter (i.e. the wave number) $\mu \in \mathbb{R}_{>0}$, a function $g \in L^2(\Omega)$, and a fixed dissipation $\epsilon = 10^{-3}$. Note that $(\bar{\cdot})$ denotes the complex conjugate of $(\cdot)$. Here the wave number μ constitutes the anticipated, and parametric, uncertainty — the term might model for instance the uncertainty in the speed of sound; the function g constitutes the unanticipated, and non-parametric, uncertainty — the term accommodates all other sources of uncertainty. We also consider a functional output:

$$\ell^{\text{out}}(w) \equiv \int_{\Gamma_1} w ds,$$

where $\Gamma_1 \equiv \{(x_1, x_2) \in \mathbb{R}^2 | \ x_1 = 0, \ x_2 \in (0, 1)\}$. We approximate the solution in a $8 \times 8 \times 2(=128$ element) triangular $\mathbb{P}^5$ finite element space, $\mathcal{U}^\mathcal{N} \subset \mathcal{U}$.

3.2. Synthetic Truths

To assess the performance of the PBDW formulation for various configurations, we consider a number of "test truths" associated with different wave numbers and two choices of the bias function g. The truth wave number $\tilde{\mu}$ takes on a value in the interval $[2, 10]$. The two bias functions $\tilde{g}$ are given by

$$\tilde{g} = \begin{cases} \tilde{g}_{\text{I}} \equiv 0, & \text{Case I} \\ \tilde{g}_{\text{II}} \equiv 0.5(\exp(-x_1) + \cos(1.3\pi x_2)), & \text{Case II}. \end{cases}$$

A given truth is defined by a particular truth parameter $\tilde{\mu}$ and bias $\tilde{g}$: $u^{\text{true}} \equiv \Upsilon_{\tilde{g}}^{\tilde{\mu}}$. We show in Figure 1 the truth fields for Case I for a few different combination of wave numbers and biases. We also show in Figure 1 the variation in $\|u^{\text{true}}\|$ as a function of the wave number $\tilde{u}$; note that there are three resonances in the parameter range considered.

3.3. Best-Knowledge Model and PBDW Spaces

We consider the parametrized best-knowledge model $G^\mu(w, v) \equiv f_{g\equiv 0}^\mu(v) - a^\mu(w, v)$ for $\mu \in \mathcal{D} \equiv [2, 10]$. The associated best-knowledge solution is $u^{\text{bk},\mu} = \Upsilon_{g\equiv 0}^\mu, \mu \in \mathcal{D}$. We then construct the background spaces $\mathcal{Z}_N$, $N = 1, \ldots, N_{\max}$, using the WEAKGREEDY_N procedure described in Algorithm 1. For simplicity, we use the dual norm of the residual as the error estimate: $\Delta_N^{\text{bk},\mu} \equiv \inf_{w \in \mathcal{Z}_N} \sup_{v \in \mathcal{U}^\mathcal{N}} |G^\mu(w, v)|/\|v\|$ (see [19] for details). The $N_{\max} = 7$ parameter points chosen by the WEAKGREEDY_N algorithm are, in order, $(10.00, 2.00, 4.50, 3.15, 6.35, 9.40, 8.65)$.

As previously discussed, the important property of $\mathcal{Z}_N$ is that it approximates the best-knowledge parametric manifold in the sense that the discretization error $\epsilon_{\text{disc},N}^{\text{bk}} \equiv \sup_{w \in \mathcal{M}^{\text{bk}}} \|w - \Pi_{\mathcal{Z}_N} w\|$ is small. We show in Figure 2 the convergence of the discretization error as a function of the dimension of N. The error decreases exponentially with N. We also note that the residual-based error estimate, $\Delta_N^{\text{bk},\mu}$, while not a rigorous bound, serves as an indicator of the true discretization error.

We now discuss the construction of the experimentally observable space $\mathcal{U}_M$. We model the (synthetic) observations by a Gaussian convolution with a standard deviation of $r_m = 0.02$: $\ell_m^{\text{o}}(\cdot) = \text{Gauss}(\cdot, x_m^c, r_m = 0.02)$. We then consider experimentally observable spaces $\mathcal{U}_M$, $M = 1, \ldots, M_{\max}$, based on two different set of observation centers $\{x_m^c\}_{m=1}^M$: randomly selected RANDOMUNIFORM_M centers and stability-maximizing SGREEDY_M centers. The first 20 centers

(a) $\Re(u^{\mathrm{true}})$: $\tilde{\mu} = 2$, $\tilde{g}_{\mathrm{I}}$ (b) $\Re(u^{\mathrm{true}})$: $\tilde{\mu} = 10$, $\tilde{g}_{\mathrm{I}}$ (c) $\Re(u^{\mathrm{true}})$: $\tilde{\mu} = 10$, $\tilde{g}_{\mathrm{II}}$
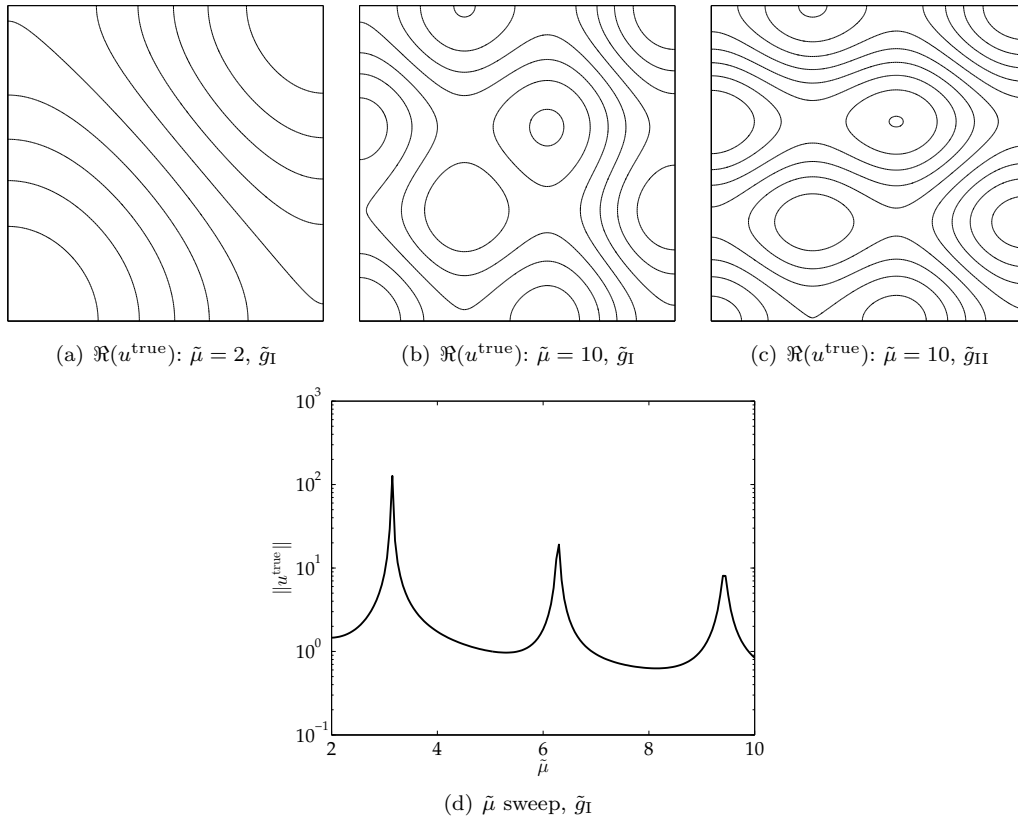

(d) $\tilde{\mu}$ sweep, $\tilde{g}_{\mathrm{I}}$

Figure 1. The truth solutions associated with the 2d Helmholtz problem.
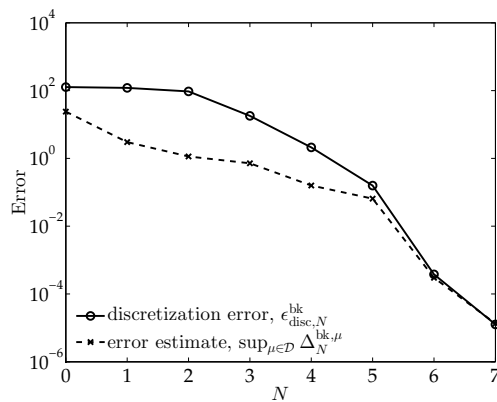
Figure 2. Convergence of the WeakGreedy$_N$ algorithm.

for each set is shown in Figure 3(a) and 3(b). We also show in Figure 3(c) an example of experimentally observable function. The function, while concentrated about $x^{\mathrm{c}}_{m=3}$, has a non-compact support; in particular, $(R_{\mathcal{U}} \ell^{\mathrm{o}}_{m=3})(x) \in [0.86, 1.45]$, $\forall x \in \Omega$, and the function does not vanish anywhere in the domain.

As previously discussed, the space $\mathcal{U}_M$ must satisfy two criteria: maximization of the stability constant $\beta_{N,M}$; the approximation of the unanticipated uncertainty space $\mathcal{Z}_N^{\perp}$. Here we focus on the assessment of the former. We shown in Figures 4(a) and 4(b) the stability constant $\beta_{N,M}$ associated with RandomUniform$_M$ and SGreedy$_M$ centers, respectively, for a few different N
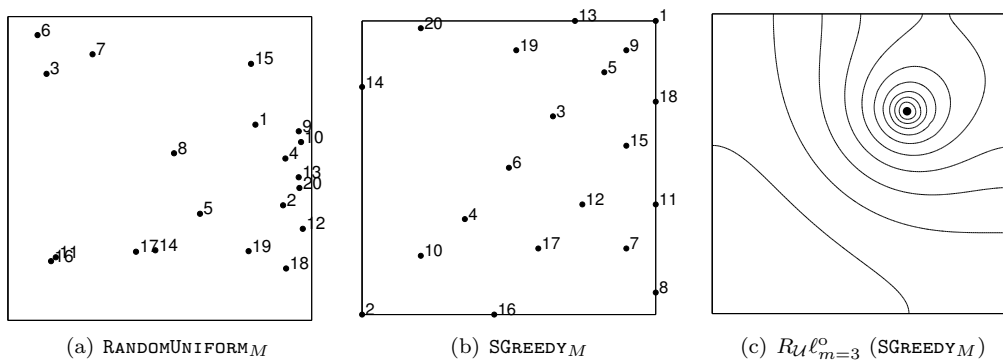
(a) RANDOMUNIFORM$_M$ (b) SGREEDY$_M$ (c) $R_{\mathcal{U}}\ell^{\mathrm{o}}_{m=3}$ (SGREEDY$_M$)

Figure 3. Observation centers selected by RANDOMUNIFORM$_{M=20}$ and SGREEDY$_{M=20}$; an experimentally observable function $R_{\mathcal{U}}\ell^{\mathrm{o}}_{m=3}$ in $\mathcal{U}_M$.
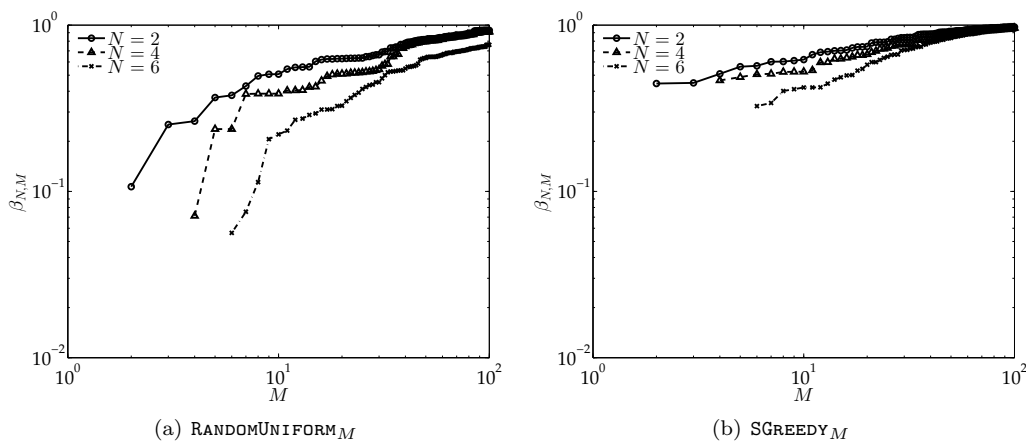

(a) RANDOMUNIFORM$_M$ (b) SGREEDY$_M$

Figure 4. Behavior of the stability constant for RANDOMUNIFORM$_M$ and SGREEDY$_M$ observation centers.

as a function of M. We observe that the SGREEDY$_M$ algorithm provides a much better stability constant in particular for a small M.

3.4. Error Analysis

3.4.1. Case I: Perfect Model. We first consider Case I: the case with a perfect best-knowledge model. As mentioned, for this case $u^{\mathrm{true}} \in \mathcal{M}^{\mathrm{bk}}$ and $u^{\mathrm{true}} = u^{\mathrm{bk},\tilde{\mu}} = \Upsilon^{\tilde{\mu}}_{g\equiv 0}$ for some $\tilde{\mu} \in \mathcal{D}$. Hence, we have no model error, $\epsilon^{\mathrm{bk}}_{\mathrm{mod}}(u^{\mathrm{true}}) = 0$; however, we still have a finite discretization error $\epsilon^{\mathrm{bk}}_{\mathrm{disc},N}$ since $\mathcal{M}^{\mathrm{bk}} \not\subset \mathcal{Z}_N$ for a finite N.

We show in Figure 5(a) the variation in the maximum relative error over the parameter domain as a function of the number of observations M for a few different values of N. For this case with a perfect model — as predicted from the *a priori* bound in Proposition 2 and the rapid convergence of the discretization error $\epsilon^{\mathrm{bk}}_{\mathrm{disc},N}$ in Figure 2 — the error decreases rapidly with N as $\epsilon^{\mathrm{bk}}_N(u^{\mathrm{true}}) \equiv \inf_{z\in\mathcal{Z}_N} \|u^{\mathrm{true}} - z\|$ decreases rapidly. Hence, the experimentally observable space $\mathcal{U}_M$, $M \geq N$, is required only to provide stability and not to complete the deficiency in the background space $\mathcal{Z}_N$ for a sufficiently large (and in practice moderate) N.

In order to understand in more detail the error behavior, we show in Figure 5(b) the convergence of the two components of the PBDW estimate: $z^*_{N,M} \in \mathcal{Z}_N$ — the background component of the estimate — and $\eta^*_{N,M} \in \mathcal{Z}^\perp_N$ — the update component of the estimate. We observe that the error in $z^*_{N,M}$ is typically smaller than the error in $\eta^*_{N,M}$. Note that this is not a contradiction with Proposition 2, which provides *bounds* for the errors in $z^*_{N,M}$ and $\eta^*_{N,M}$.

(a) state error

(b) η_N^* and z_N^* error

(c) fraction anticipated

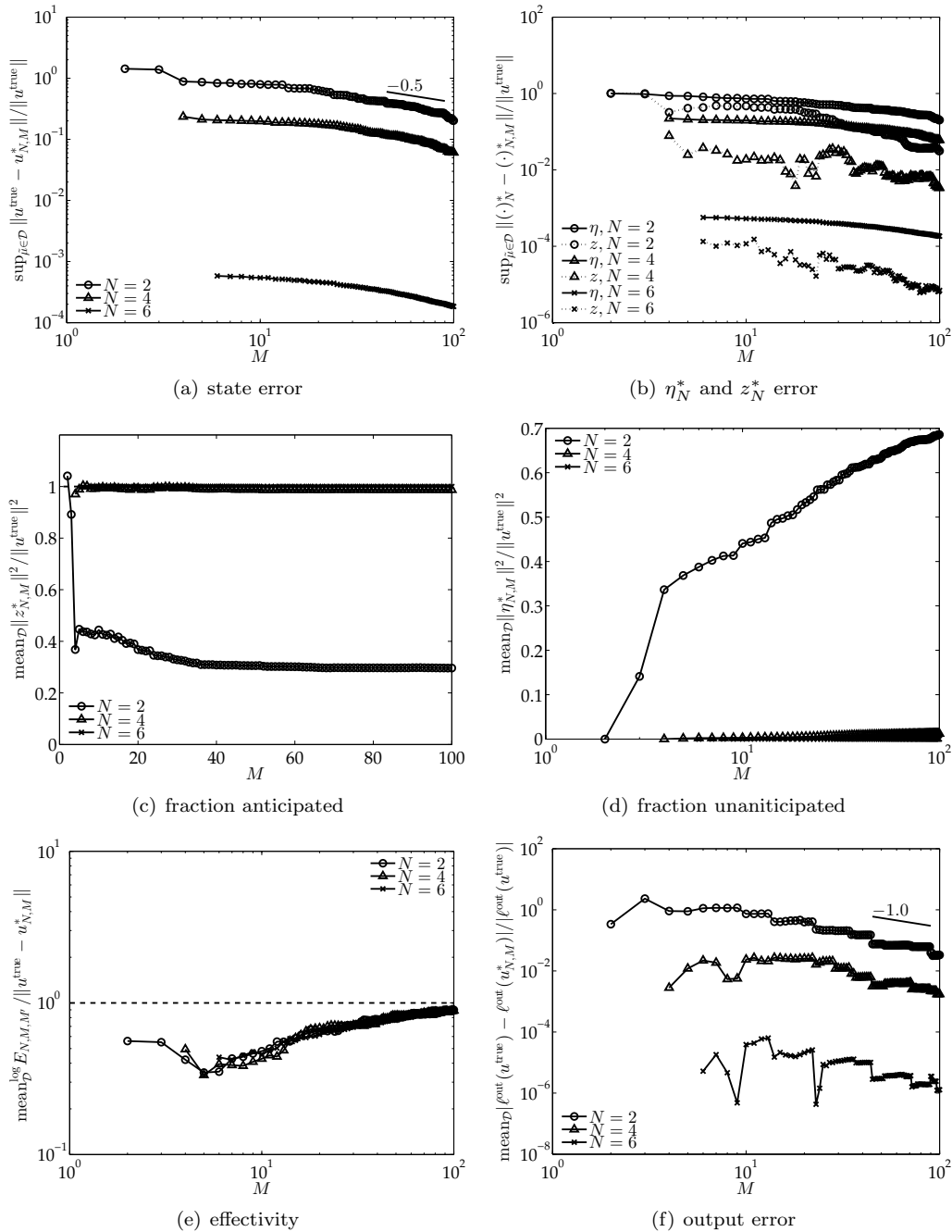(d) fraction unaniticipated

(e) effectivity

(f) output error

Figure 5. Case I. Behavior of the maximum relative error over the parameter domain, the maximum error for the update and background components, the anticipated and unanticipated fractions of the state, the log-mean *a posteriori* error estimate effectivity (for $M' = 2M$), and the mean relative output error as a function of the number of observations M for a few different values of N using SGREEDY$_M$ observation centers.

We in addition show in Figures 5(c) and 5(d) the fraction of the state anticipated and unanticipated, respectively, by the parametrized best-knowledge model. As there is no model error ($\epsilon_{\mathrm{mod}}^{\mathrm{bk}}(u^{\mathrm{true}}) = 0$), the unanticipated fraction vanishes as $N \to \infty$.

We show in Figure 5(e) the variation in the *a posteriori* error estimate effectivity, $E_{N,M,M'}/\|u^{\mathrm{true}} - u_{N,M}^*\|$, as a function of M and N for $M' = 2M$. The error estimate

unfortunately underestimates the true error. However, the effectivity approaches unity as M (and hence M') increases.

We finally show in Figure 5(f) the convergence of the PBDW output estimates. As we have observed for the $\| \cdot \|$-norm of the error, we observe a rapid convergence of the output error with N for this case with a perfect model. In addition, as predicted by Proposition 3, we observe superconvergence with M: the output error decreases as M^{-1} as opposed to $M^{-1/2}$ for the state error.

3.4.2. Case II: Imperfect Model. We now consider the truths u^{true} with $\tilde{g} = \tilde{g}_{\text{II}} \neq 0$ such that the parametrized best-knowledge model based on $\tilde{g} \equiv 0$ is inconsistent with the truths. In other words, the model error $\epsilon_{\text{mod}}^{\text{bk}}(u^{\text{true}}) \neq 0$ and $u^{\text{true}} \notin \mathcal{M}^{\text{bk}}$. Proposition 2 predicts that, since $\epsilon_N^{\text{bk}}(u^{\text{true}}) \equiv \inf_{z \in \mathcal{Z}_N} \|u^{\text{true}} - z\|$ does not converge to 0, we must rely on the relatively slow convergence with M provided by $\inf_{q \in \mathcal{U}_M \cap \mathcal{Z}_N^{\perp}} \|\Pi_{\mathcal{Z}_N^{\perp}} u^{\text{true}} - q\|$. Figure 6(a) confirms that this indeed is the case; while the error decreases with N, the decrease is not as rapid as that observed for the perfect model in Case I. We observe that the error converges at the rate of $M^{-1/2}$, and in fact we must rely on this rather slow convergence, and not the rapid convergence with N, to obtain a good estimate.

We observe in Figure 6(b) that, in the case of imperfect models, the error in $\eta_{N,M}^*$ dominates over the error in $z_{N,M}^*$. This is consistent with the fact that $\|\eta_N^*\|$ does not decrease rapidly with N for an imperfect model. We confirm in Figures 6(c) and 6(d) that this indeed is the case: since model error $\epsilon_{\text{mod}}^{\text{bk}}(u^{\text{true}}) \neq 0$, the fraction of the state unanticipated by the parametrized best-knowledge model does not vanish even if $N \to \infty$. We show in Figure 6(e) that the *a posteriori* error estimate in Case II works as well as it does in Case I. We finally observe in Figure 6(f) that the output error, like the state error, does not decrease rapidly with N, but, unlike the state error, superconverges with M at the rate of M^{-1}.

We finally assess the effect of observation centers on the state estimates. We show in Figure 7(a) the convergence of the state estimation error using the RANDOMUNIFORM$_M$ observation centers. Compared to the results shown in Figure 5(a) obtained using the SGREEDY$_M$ observation centers, we observe an increase in the error in particular for a small M. To understand the cause of the increased error, we show in Figure 7(b) the decomposition of the error into the background and update components; we then compare the results with that shown in Figure 5(b) obtained using the SGREEDY$_M$ observation centers. We note that in general the error in the update component $\eta_{N,M}^*$ is not strongly affected by the choice of the observation centers; this is consistent with Proposition 2 which states that the estimation of η_N^* is independent of the stability constant $\beta_{N,M}$, which strongly depends on the observation centers as shown in Figures 4(a) and 4(b). On the other hand, we note that the error in the background component $z_{N,M}^*$ is much larger for the RANDOMUNIFORM$_M$ observation centers than for the SGREEDY$_M$ observation centers, especially for a small M. This again is consistent with Proposition 2 which shows that the stability constant $\beta_{N,M}$ plays a crucial role in the estimation of z_N^*.

4. PHYSICAL PROBLEM: RAISED-BOX ACOUSTIC RESONATOR

4.1. Physical System

We now consider the application of the PBDW framework to a physical system: a raised-box acoustic resonator. In particular, we wish to estimate the (time-harmonic) pressure field inside the raised-box acoustic resonator described as a complex field in the frequency domain.

We show in Figure 8(a) the physical system: a five-sided, raised, acrylic box is separated from a bottom panel by a small gap that permits acoustic radiation from the raised box interior to the exterior; a speaker (Tang Band W2-1625SA) mounted in the center of one side of the box provides a sound source at a single prescribed frequency f^{dim}. We show in Figure 8(b) the

(a) state estimation error

(b) η_N^* and z_N^* error

(c) fraction anticipated

(d) fraction unaniticipated
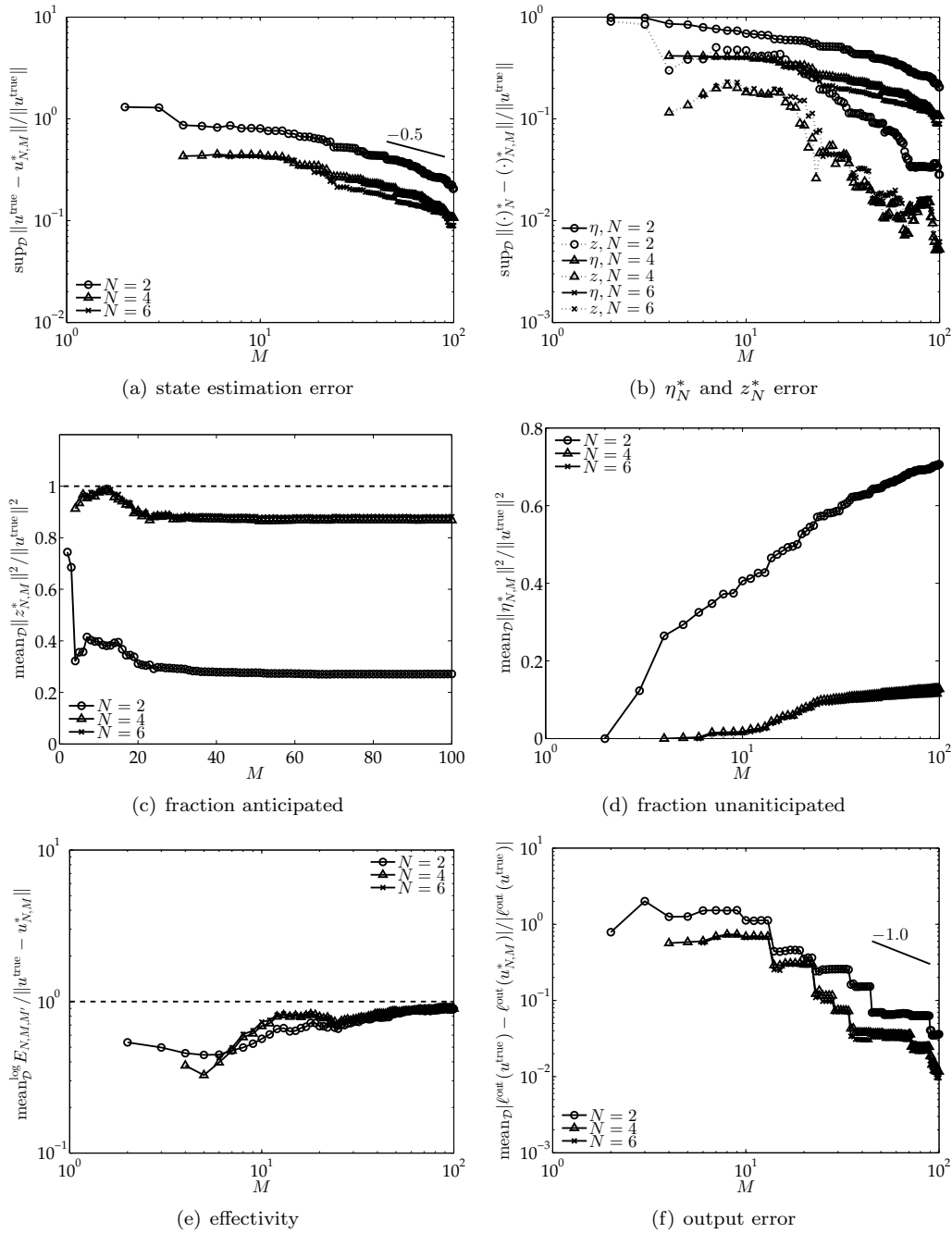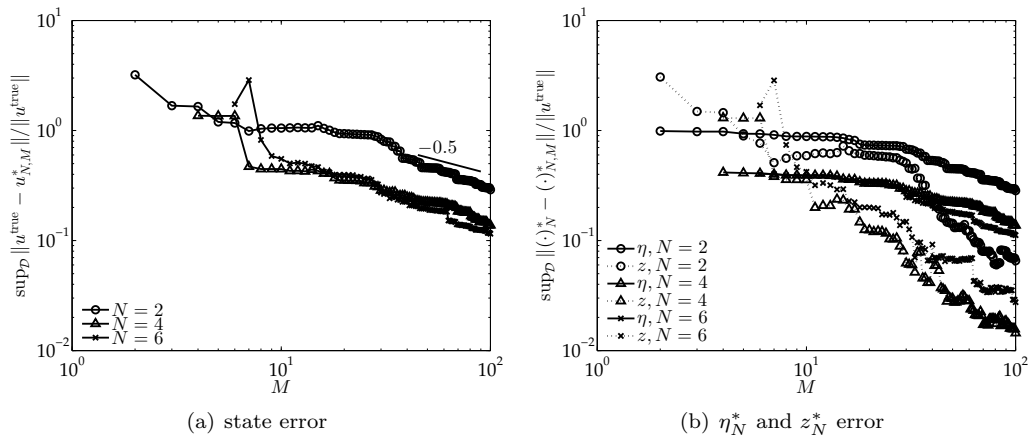

(e) effectivity

(f) output error

Figure 6. Case II. Behavior of the maximum relative error over the parameter domain, the maximum error for the update and background components, the anticipated and unanticipated fractions of the state, the log-mean *a posteriori* error estimate effectivity (for $M' = 2M$), and the mean relative output error as a function of the number of observations M for a few different values of N using SGREEDY_M observation centers.

dimensional values (superscript "dim") of the geometric and thermodynamic variables that define the physical system.

4.2. Robotic Observation Platform.

(a) state error
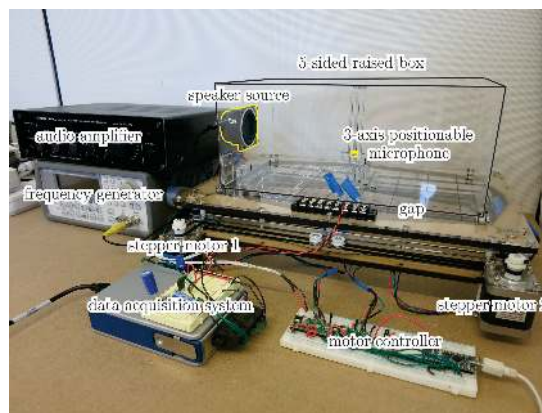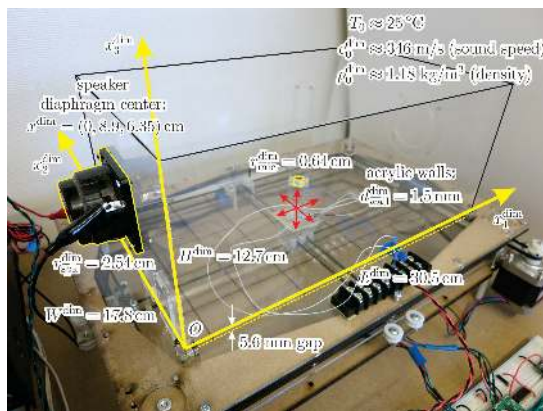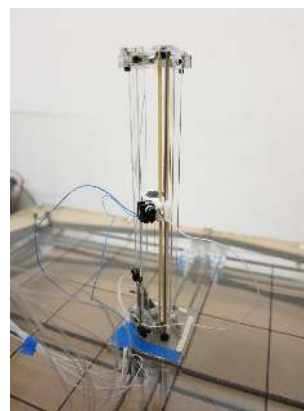
(b) η_N^* and z_N^* error

Figure 7. Case II. Behavior of the maximum relative error over the parameter domain and the maximum error for the update and background components as a function of the number of observations M for a few different values of N using RANDOMUNIFORM$_M$ observation centers.

(a) robotic observation platform

(b) raised-box acoustic resonator

(c) microphone holder

Figure 8. Configuration of the robotic observation platform and the raised-box acoustic resonator.

4.2.1. Data Acquisition. To permit autonomous, rapid, and accurate data acquisition, we design and build a robotic observation platform for the raised-box acoustic resonator.
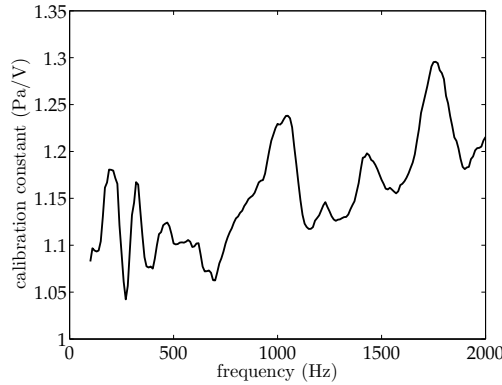
Figure 9. Measured calibration curve of the microphone (Radio Shack model 270-092) and preamplifier.

As shown in Figure 8(a), a microphone (Radio Shack model 270-092) attached to a 3-axis positionable holder measures the pressure at a specified position inside the raised box. Actuation of the microphone in the x_1 and x_2 directions (as defined in Figure 8(b)) is provided by two stepper motors controlling a belt-driven output (not shown) that is magnetically coupled to the microphone holder shown in Figure 8(c) through the bottom panel. Actuation of the microphone in the x_3 direction is provided by a small DC motor mounted to the microphone holder that positions the microphone via potentiometer position feedback.

Figure 8(a) also shows the frequency generator and audio amplifier used to control the output of the speaker, the motor controller used to control the stepper and DC motors, and the data acquisition system used to capture the measured speaker input and microphone output.

A typical experiment consists of positioning the microphone in three dimensions, generating a sequence of tones at prescribed frequencies using the frequency generator, amplifier, and speaker, and recording the speaker input and microphone output using the data acquisition system. The microphone is then repositioned and the process is repeated.

Prior to use, the microphone was calibrated over the frequency range of interest using a sound level calibrator (Reed SC-05) accurate to within 6%, sound level meter (Extech 407730), and a reference microphone (Dayton Audio EMM-6) with a known frequency response accurate to within 1%. The measured calibration curve of the microphone and its custom microphone preamplifier circuit is shown in Figure 9.

4.2.2. Data Reduction. We briefly discuss our data reduction procedure. We focus here on the data reduction of a single speaker-microphone observation pair; to obtain M observations, we repeat the procedure M times.

The microphone generates a voltage signal $\varphi_{\mathrm{mic}}^{\mathrm{dim}}(x^{\mathrm{dim}}, t^{\mathrm{dim}})$ as a function of time t^{dim} at a given location x^{dim} within the box. We then assume that the measured voltage is of the form $\varphi_{\mathrm{mic}}^{\mathrm{dim}}(x^{\mathrm{dim}}, t_j^{\mathrm{dim}}) = \Re\left\{ \Phi_{\mathrm{mic}}^{\mathrm{dim}}(x^{\mathrm{dim}}; f^{\mathrm{dim}}) e^{i2\pi f^{\mathrm{dim}} t_j^{\mathrm{dim}}} \right\} + \epsilon_{\mathrm{mic}}^{\mathrm{dim}}(x^{\mathrm{dim}}, t_j^{\mathrm{dim}}), \ j = 1, \ldots, M',$ where $\Phi_{\mathrm{mic}}^{\mathrm{dim}}(x^{\mathrm{dim}}; f^{\mathrm{dim}}) \in \mathbb{C}$ is the complex microphone voltage, $\epsilon_{\mathrm{mic}}^{\mathrm{dim}}(x^{\mathrm{dim}}, t_j^{\mathrm{dim}}) \in \mathbb{R}$ is the noise, and M' is the number of measurements in the time series. We take $M' = 4{,}000$ measurements in our experiment. We then assume that $\epsilon_{\mathrm{mic}}^{\mathrm{dim}}(x^{\mathrm{dim}}, t^{\mathrm{dim}}) \sim \mathcal{N}(0, (\sigma_{\mathrm{mic}}^{\mathrm{dim}}(x^{\mathrm{dim}}; f^{\mathrm{dim}}))^2)$ and perform linear regression to identify the complex microphone voltage $\Phi_{\mathrm{mic}}^{\mathrm{dim}}(x^{\mathrm{dim}}; f^{\mathrm{dim}}) \in \mathbb{C}$ and the noise standard deviation $\sigma_{\mathrm{mic}}^{\mathrm{dim}}(x^{\mathrm{dim}}) \in \mathbb{R}_{>0}$.

We apply a similar data reduction procedure to the speaker voltage signal $\varphi_{\mathrm{spk}}^{\mathrm{dim}}(f^{\mathrm{dim}})$ to deduce the complex speaker velocity $\Phi_{\mathrm{spk}}^{\mathrm{dim}}(f^{\mathrm{dim}}) \in \mathbb{C}$ and the associated standard deviation $\sigma_{\mathrm{spk}}^{\mathrm{dim}}(f^{\mathrm{dim}}) \in \mathbb{R}_{>0}$. We emphasize that we measure the microphone voltage $\varphi_{\mathrm{mic}}^{\mathrm{dim}}(x^{\mathrm{dim}}, t^{\mathrm{dim}})$ and the speaker voltage $\varphi_{\mathrm{spk}}^{\mathrm{dim}}(t^{\mathrm{dim}})$ simultaneously over the same time period; we appeal to this simultaneous data acquisition to deduce the phase information of the pressure signal from a single microphone observation as described shortly.
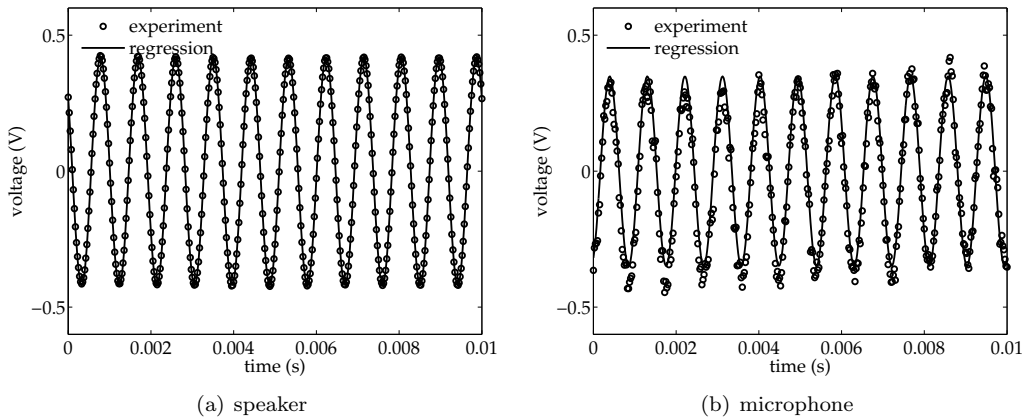
(a) speaker   (b) microphone

Figure 10. A time trace of typical raw data and regression estimate over the first 0.01s; the data acquisition period is 10 times longer. ($x^{\mathrm{dim}} = (27.9, 15.2, 1.3)$cm, $\tilde{f}^{\mathrm{dim}} = 1100$Hz)

Once we obtain the speaker-microphone voltage pair $(\Phi_{\mathrm{spk}}^{\mathrm{dim}}, \Phi_{\mathrm{mic}}^{\mathrm{dim}})$, we calculate the associated speaker velocity and microphone pressure. We model the speaker as a harmonic oscillator to identify the (frequency-dependent) transfer function from the applied speaker voltage $\Phi_{\mathrm{spk}}^{\mathrm{dim}}$ to the resultant speaker velocity $V_{\mathrm{spk}}^{\mathrm{dim}}$; the construction of the transfer function is discussed in Section 4.3. We convert the microphone voltage $\Phi_{\mathrm{mic}}^{\mathrm{dim}}$ to the associated pressure $P_{\mathrm{mic}}^{\mathrm{dim}}$ using the calibration curve shown in Figure 9.

We finally introduce the following normalized quantities: the coordinate $x \equiv x^{\mathrm{dim}}/r_{\mathrm{spk}}^{\mathrm{dim}}$; the frequency $k \equiv 2\pi f^{\mathrm{dim}} r_{\mathrm{spk}}^{\mathrm{dim}}/c_0^{\mathrm{dim}}$; the complex pressure $u \equiv (P^{\mathrm{dim}}/V_{\mathrm{spk}}^{\mathrm{dim}})/(\rho_0^{\mathrm{dim}} c_0^{\mathrm{dim}})$. Here ρ_0^{dim} is the density of the air and c_0^{dim} is the speed of sound. Under this normalization, the microphone centered at x_m^{c} effectively provides a local average of u in the vicinity of x_m^{c}; this observed normalized pressure is given by $P^{\mathrm{obs}}(x_m^{\mathrm{c}}; k) \equiv (P_{\mathrm{mic}}^{\mathrm{dim}}(x_m^{\mathrm{c}}; f^{\mathrm{dim}})/V_{\mathrm{spk}}^{\mathrm{dim}}(f^{\mathrm{dim}}))/(\rho_0^{\mathrm{dim}} c_0^{\mathrm{dim}}) \in \mathbb{C}$. Note that, in our normalization of the pressure, the initial (arbitrary) phase angle of the (complex) speaker velocity cancels out (and subsequently becomes irrelevant) as it appears in P^{dim} in the numerator and $V_{\mathrm{spk}}^{\mathrm{dim}}$ in the denominator. It is important to note that we may thus obtain phase information throughout the pressure field with just a single microphone, a substantial advantage in the real-time context as implemented in our robotic observation platform. We shall exploit phase as a sensitive error metric for our data assimilation procedure.

We comment on the precision of typical experimental data. We show in Figure 10 a time trace of typical regression for the speaker and microphone. The estimate of the complex amplitude for the speaker voltage is $0.266 + 0.324i$V and the associated standard deviation is 0.00095V; the signal-to-noise ratio is 443. The estimate of the complex amplitude for the microphone voltage is $-0.319 - 0.140i$V and the associated standard deviation is 0.00185V; the signal-to-noise ratio is 189. Note that because for a given frequency the voltage-to-pressure calibration is linear, the signal-to-noise ratio of the voltage directly applies to the pressure. We conclude that the noise associated with any given observation is small. In addition, because the signal-to-noise ratio of the speaker voltage, which is used in normalization, is high, we expect the normalized pressure u to inherit this signal-to-noise ratio.

We continue the assessment of the precision of the data, in particular reproducibility and environmental control, through a repetition test. We show in Figure 11 typical normalized pressure observed in two different experiments. The microphone was moved to the location following two different paths; hence, the comparison captures any hysteresis that might be present in the microphone positioning system. We observe that the two results closely match each other. The comparison suggests that the physical pressure field is invariant in the sense that within a given set of observations we maintain environmental conditions such as the
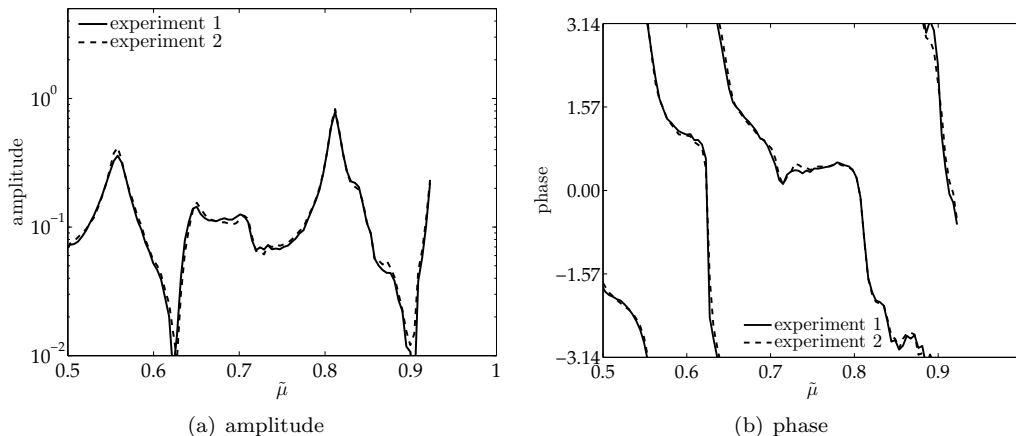
(a) amplitude   (b) phase

Figure 11. Comparison of two the normalized pressures obtained in two different experiments ($x^{\text{dim}} = (27.9, 15.2, 1.3)$cm)

temperature.

The calibration of Section 4.2.1 ensures accurate microphone pressure measurement; the regression results and associated signal-to-noise ratio suggest very little noise associated with the (effectively) Fourier transform of the temporal signal; and finally the repetition test indicates good control of position and environmental conditions and hence very little systematic error. As regards the latter, we also note that the microphone dimension is small compared to the wavelength of the acoustic waves, and hence any sufficiently small choice for r_m suffices; we further note that the instrument holder of Figure 8(c) is largely acoustically invisible in particular due to the thin profile and light vertical-drive mechanism.

We conclude that for our purposes here (i) we may indeed apply the "noise-free" observation framework developed in the previous sections, and (ii) for purposes of assessment, we may equate our experiments to the true field.

4.2.3. Dataset. We consider 92 configurations associated with the frequency of $\tilde{f}^{\text{dim}} = 1090, \ldots, 2000$ Hz; the associated normalized frequency based on the ambient temperature, $\tilde{k} = \tilde{\mu}$, takes on a value in $[0.502, 0.921]$. We acquire data at 84 spatial points distributed on a Cartesian grid:

$$x_m^{\text{c}} \in \Xi \equiv \{1.00, 2.67, 4.33, 6.00, 7.67, 9.33, 11.00\} \times \{1.00, 2.67, 4.33, 6.00\} \times \{0.50, 2.50, 4.50\}.$$

We then apply the data reduction procedure described above to compute $P^{\text{obs}}(x_m^{\text{c}}; \tilde{\mu})$.

We recall that the regression analysis and repeatability test suggest that the noise in the pressure observations is in fact small. We hence employ the dataset for two purposes. First, we use the dataset as experimental observations from which to construct the PBDW estimate; in fact, because the noise is small, we may apply the noise-free formulation and theory developed in Section 2. Second, we use the dataset as a surrogate for the truth with which to assess the accuracy of the PBDW estimate $P^{\text{true}}(x_m^{\text{c}}; \tilde{\mu}) \equiv P^{\text{obs}}(x_m^{\text{c}}; \tilde{\mu})$; we recall that our goal is prediction of the true state, and not just the experimental observations — the two coincide only in the noise-free case.

4.3. Best-Knowledge Model

The geometry of the mathematical model is shown in Figure 12. We recall that our goal is to approximate the pressure field everywhere inside the raised box, Ω. We in addition introduce a superdomain for the best-knowledge model, $\Omega^{\text{bk}} \supset \Omega$, that includes the regions both inside and outside of the box such that we may model the radiation from the bottom gap of the box.
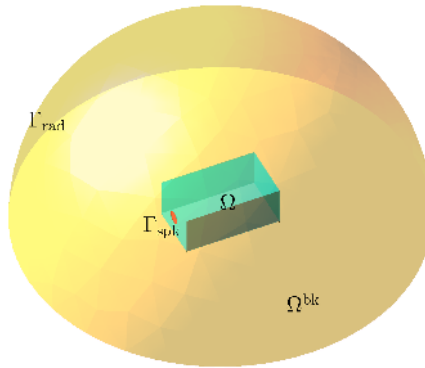
Figure 12. Geometry of the computational model. Here, Ω is the domain inside of the raised box, Ω^{bk} is the (extended) computational domain that includes the regions inside and outside of the raised-box, Γ_{spk} is the speaker boundary, and Γ_{rad} is the radiation boundary.

We then introduce a Hilbert space $\mathcal{U}$ over Ω endowed with a weighted H^1 inner product and norm:

$$(w, v) \equiv \int_\Omega \nabla w \cdot \nabla \bar{v} dx + \kappa^2 \int_\Omega w \bar{v} dx \quad \text{and} \quad \|w\| \equiv \sqrt{(w, w)}$$

for a reference wavenumber $\kappa = 0.5$. The reference wavenumber is chosen to induce an update function $q_m \equiv R_{\mathcal{U}_M} \ell_m^{\mathrm{o}}$ with a spatial decay on the order of the wavelength.

We define the extended parametrized best-knowledge solution over Ω^{bk} by a weak statement: find $u^{\mathrm{bk},\mu} \in \mathcal{U}^{\mathrm{bk}} \equiv H^1(\Omega^{\mathrm{bk}})$ such that

$$G^\mu(u^{\mathrm{bk},\mu}, v) \equiv f^\mu(v) - a^\mu(u^{\mathrm{bk}}, v) = 0 \quad \forall v \in \mathcal{U}^{\mathrm{bk}}$$

where

$$a^\mu(w, v) \equiv \int_\Omega \nabla w \cdot \nabla \bar{v} dx - \mu^2 \int_\Omega w \bar{v} dx + \left(i\mu + \frac{1}{R} \right) \int_{\Gamma_{\mathrm{rad}}} w \bar{v} ds \quad \forall w, v \in \mathcal{U},$$

$$f^\mu(v) \equiv i\mu \int_{\Gamma_{\mathrm{spk}}} 1 \cdot 1 \bar{v} ds \quad \forall v \in \mathcal{U}.$$

We model the harmonic excitation generated by the speaker by a uniform Neumann condition over Γ_{spk}; note that, under our normalization, the speaker velocity is unity. We model the radiation into free space by a first-order accurate radiation boundary condition on Γ_{rad}. The parameter domain associated with the wave number is $\mathcal{D} = [0.5, 1.0]$. Thanks to the radiation term, the problem is well posed for any $\mu \in \mathcal{D}$. We approximate the solution in a 35,325-element $\mathbb{P}^3$ finite element space.

We briefly discuss our speaker model. We model the speaker as a harmonic oscillator driven by an electromagnetic voice coil. The frequency-dependent transfer function of the speaker diaphragm velocity $V_{\mathrm{spk}}^{\mathrm{dim}}$ with respect to the speaker input voltage $\Phi_{\mathrm{spk}}^{\mathrm{dim}}$ in terms of the voice coil BL product $(BL)_{\mathrm{spk}}^{\mathrm{dim}}$, the voice coil electrical resistance $R_{\mathrm{e,spk}}^{\mathrm{dim}}$, the voice coil electrical inductance $L_{\mathrm{e,spk}}^{\mathrm{dim}}$, the speaker suspension stiffness $k_{\mathrm{spk}}^{\mathrm{dim}}$, the speaker moving mass $m_{\mathrm{spk}}^{\mathrm{dim}}$, and the speaker mechanical damping $b_{\mathrm{spk}}^{\mathrm{dim}}$ is then given by

$$\frac{V_{\mathrm{spk}}^{\mathrm{dim}}}{\Phi_{\mathrm{spk}}^{\mathrm{dim}}} = \frac{(BL)_{\mathrm{spk}}^{\mathrm{dim}} i 2\pi f^{\mathrm{dim}}}{\left(R_{\mathrm{e,spk}}^{\mathrm{dim}} + i 2\pi f^{\mathrm{dim}} L_{\mathrm{e,spk}}^{\mathrm{dim}} \right) \left(k_{\mathrm{spk}}^{\mathrm{dim}} - m_{\mathrm{spk}}^{\mathrm{dim}} \left(2\pi f^{\mathrm{dim}} \right)^2 + i 2\pi f^{\mathrm{dim}} b_{\mathrm{eff,spk}}^{\mathrm{dim}} \right)}$$
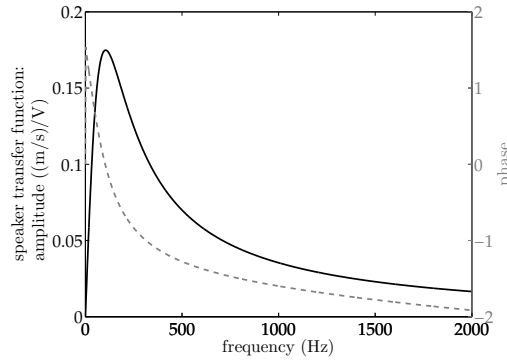
Figure 13. Speaker (Tang Band W2-1625SA) transfer function (magnitude and phase) for the measured parameter values.

Table I. Manufacturer specified and measured speaker parameters

parameter	specified value	measured value	units
$R_{\text{e,spk}}^{\text{dim}}$	6.6	7.2	Ohm
$L_{\text{e,spk}}^{\text{dim}}$	2.15×10^{-4}	2.64×10^{-4}	Henry
$(BL)_{\text{spk}}^{\text{dim}}$	5.16	5.4	T·m
$k_{\text{spk}}^{\text{dim}}$	772.2	1410.8	N/m
$m_{\text{spk}}^{\text{dim}}$	2.3×10^{-3}	3.4×10^{-3}	kg
$b_{\text{spk}}^{\text{dim}}$	0.05	0.24	N·s/m

where we define the effective damping of the speaker as

$$b_{\text{eff,spk}}^{\text{dim}} = b_{\text{spk}}^{\text{dim}} + \frac{\left((BL)_{\text{spk}}^{\text{dim}}\right)^2}{R_{\text{e,spk}}^{\text{dim}} + i2\pi f^{\text{dim}} L_{\text{e,spk}}^{\text{dim}}}.$$

Experiments were conducted to measure the various speaker parameters, yielding values which differ from the manufacturer specified values. Both sets of values are listed in Table I. The transfer function of the speaker for the measured parameter values is shown in Figure 13.

4.4. PBDW Spaces

4.4.1. Background Spaces $\mathcal{Z}_N$. We employ the superdomain formulation described in Section 2.7.3. We first apply the Week Greedy algorithm described in Algorithm 1 to form $\text{WEAKGREEDY}_N(\mathcal{M}^{\text{bk}}) \to \mathcal{Z}_N^{\text{bk}}$, $N = 1, \ldots, 15 \equiv N_{\max}$. We then restrict the functions in $\mathcal{Z}_N^{\text{bk}}$ to the domain of interest to form $\mathcal{Z}_N = \{z \in \mathcal{U} | z = z^{\text{bk}}|_\Omega, z^{\text{bk}} \in \mathcal{Z}_N^{\text{bk}}\}$. We emphasize that $\mathcal{Z}_N \subset \mathcal{U}$ is defined over Ω, not the (extended) best-knowledge domain Ω^{bk}.

4.4.2. Experimentally Observable Update Spaces $\mathcal{U}_M$. We model the experimental observations provided by the microphone with Gaussians. Specifically, we consider $\ell_m^{\text{o}}(\cdot) = \text{Gauss}(\cdot; x_m^{\text{c}}, r_m = 0.2)$. We choose a standard deviation r_m that is consistent with an approximate filter width of the microphone; however, because the spatial extend of the microphone is small compared to the pressure wavelength, the precise choice of r_m is not too important. The observation points are specified by a version of the stability maximization algorithm, $\text{SGREEDY}_M^{\text{d}}$, modified to accommodate a discrete set of observation points. Namely, we replace Step 5 of Algorithm 2 by

$$x^* = \arg\sup_{x \in \Xi} |\text{Gauss}(w_{\text{inf}} - v_{\text{sup}}; x, r_m = 0.2)|;$$

we thus guarantee that the observation points are in Ξ and hence the associated data is in the dataset. We then obtain $\mathcal{U}_M = \text{SGREEDY}_M^{\text{d}}(\mathcal{Z}_{N_{\max}})$, $M = 1, \ldots, 48 \equiv M_{\max}$.
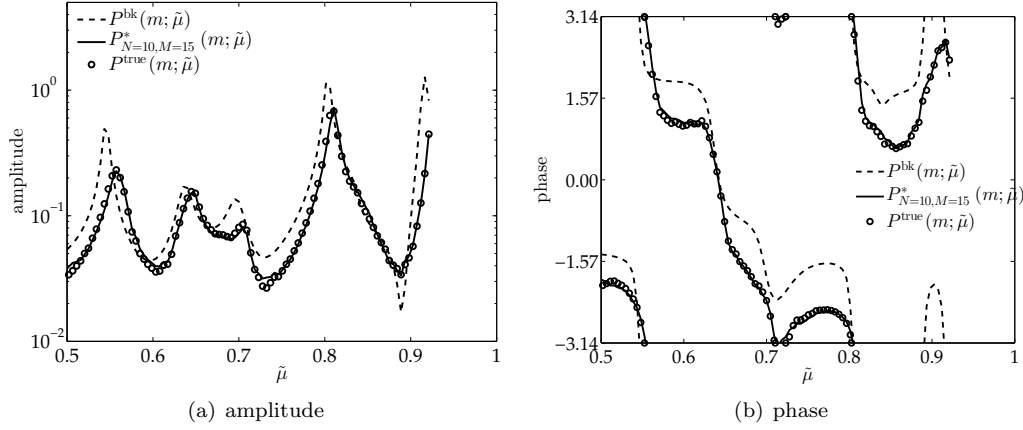
(a) amplitude (b) phase

Figure 14. Measured (experiment) and predicted (best-knowledge $u^{\mathrm{bk}}_{\tilde{\mu}}$ and PBDW estimate $u^*_{N=10,M=15}$) frequency responses at $x^{\mathrm{c}}_m = (9.33, 2.67, 4.50)$.

4.5. Real-Time In-Situ Data Assimilation

We briefly summarize the timing associated with the online data acquisition and data assimilation. The robotic observation platform requires approximately 3 seconds per observation to reposition the microphone and to take the pressure measurement. The solution of the PBDW saddle system requires less than 0.1 milliseconds on a laptop. The total online time is thus dictated by the time for online data acquisition and is approximately $3M$ seconds, where M is the number of observations.

4.6. Assessment

We compare the predicted and observed (complex) pressure at 36 assessment points not chosen by the $\mathtt{SGREEDY}^{\mathrm{d}}_{M=48}$ procedure: $\Xi^{\mathrm{a}} = \Xi \setminus \Xi_{\mathtt{SGREEDY}^{\mathrm{d}}_{M=48}}$. We shall compare the best-knowledge estimate, the PBDW estimate, and the truth defined by

$$P^{\mathrm{bk}}(m; \tilde{\mu}) = \mathrm{Gauss}(u^{\mathrm{bk},\mu=\tilde{\mu}}; x^{\mathrm{c,a}}_m, 0.2)$$

$$P^*_{N,M}(m; \tilde{\mu}) = \mathrm{Gauss}(u^*_{N,M}; x^{\mathrm{c,a}}_m, 0.2)$$

$$P^{\mathrm{true}}(m; \tilde{\mu}) = \{\text{normalized experimental pressure observation for mic at } x = x^{\mathrm{c,a}}_m\}$$

$$\equiv \mathrm{Gauss}(u^{\mathrm{true}}; x^{\mathrm{c,a}}_m),$$

respectively. Note that $\tilde{\mu}$ is not in any way utilized in the PBDW data assimilation process; the $\tilde{\mu}$ argument in $P^*_{N,M}(m; \tilde{\mu})$ is a label for the particular set of observations which inform the state estimation procedure.

A typical frequency response obtained at an assessment point is shown in Figure 14. The PBDW estimate, using a $N = 10$ background space and $M = 15$ experimental observations, provides a more accurate prediction of the truth than the best-knowledge estimate.

To assess the behavior of the PBDW estimate in more detail, we show in Figure 15 the variation in the (normalized) ℓ^2 norm of the error over Ξ^{a},

$$\mathcal{E}^{\mathrm{a}}_{\mathrm{avg}} \equiv \left(\frac{1}{M^{\mathrm{a}}} \sum_{m=1}^{M^{\mathrm{a}}} |l^{\mathrm{obs}}_m - \ell^{\mathrm{o}}_m(\cdot)|^2 \right)^{1/2},$$

as a function of the dimension of the background space N and the number of observations M at select frequencies. We recall that $M^{\mathrm{a}} = |\Xi^{\mathrm{a}}| = 36$ and the assessment set provides a good coverage of the domain Ω; hence the discrete sum serves as an approximation of the $L^2(\Omega)$ error. We observe that the error decreases rapidly with N and slowly (but steadily) with M.
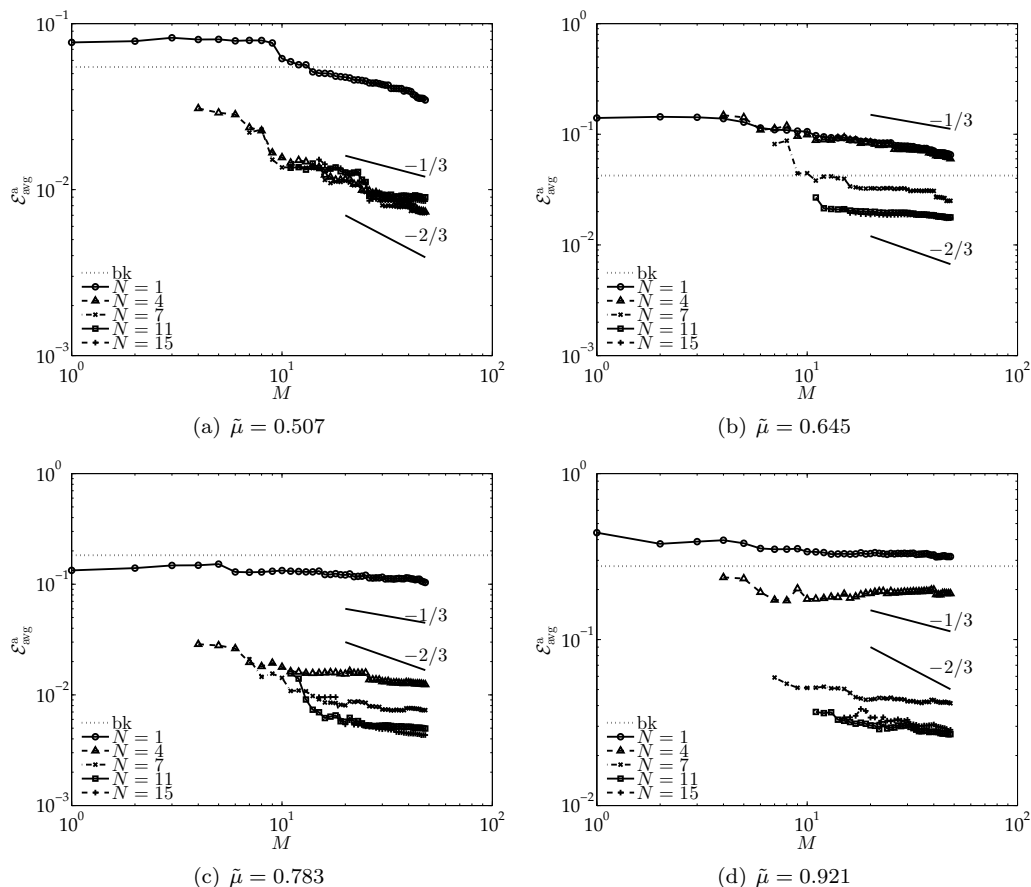
(a) $\tilde{\mu} = 0.507$

(b) $\tilde{\mu} = 0.645$

(c) $\tilde{\mu} = 0.783$

(d) $\tilde{\mu} = 0.921$

Figure 15. The variation in the error with the background-space dimension N and the number of observations M at four different frequencies.

We finally compare, similar to the synthetic case, the results obtained using two different sets of observation points: the points selected by the $\texttt{SGreedy}_M^{\mathrm{d}}$ and $\texttt{RandomUniform}_M^{\mathrm{d}}$. We compare the estimated errors in Figures 16(a) and 16(b); we observe that the error is smaller for $\texttt{SGreedy}_M^{\mathrm{d}}$ than for $\texttt{RandomUniform}_M^{\mathrm{d}}$, especially when M is close to N. We then compare the stability constants in Figures 16(c) and 16(d); we observe that the $\texttt{SGreedy}_M^{\mathrm{d}}$ provides better stability than $\texttt{RandomUniform}_M^{\mathrm{d}}$, and this likely results in the improved state estimate. We hence conclude that, even in the real data setting, we benefit from the algorithms informed by the theory developed in the weak variational framework.

REFERENCES

1. J. Antoni. A Bayesian approach to sound source reconstruction: optimal basis, regularization, and focusing. *J. Acoust. Soc. Am.*, 131:2873–2890, 2012.
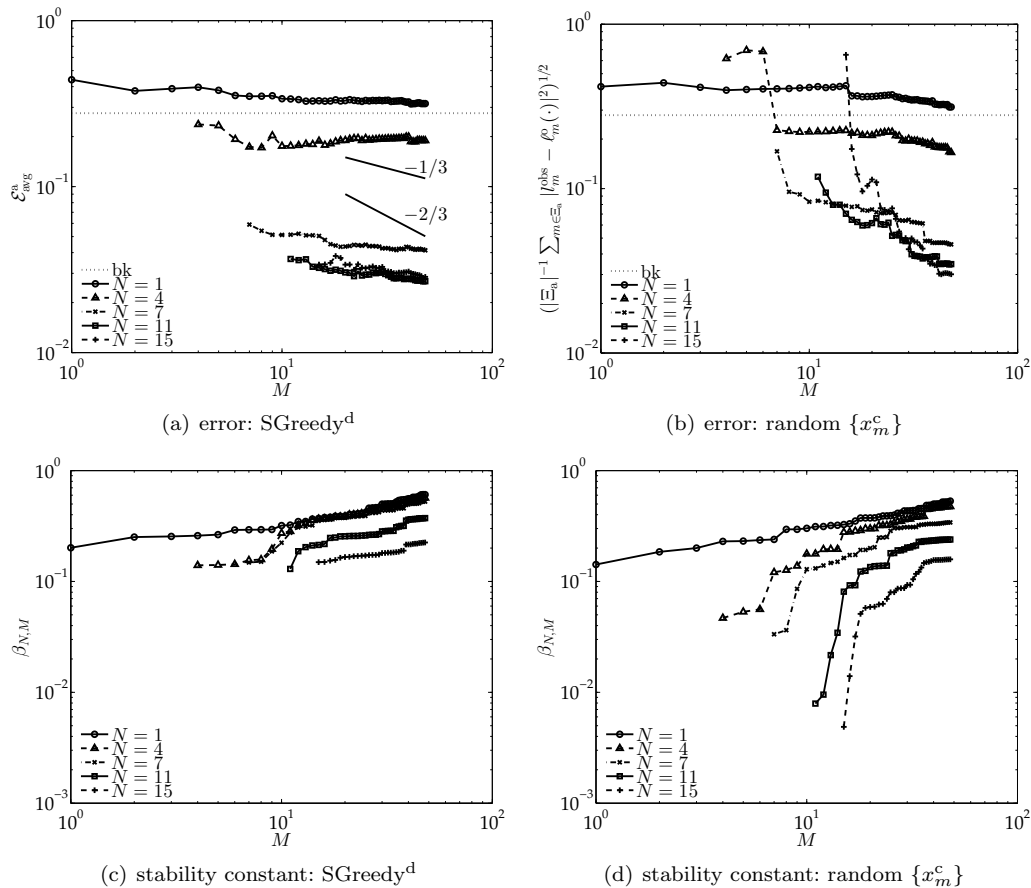
(a) error: SGreedy$^{\mathrm{d}}$

(b) error: random $\{x_m^{\mathrm{c}}\}$

(c) stability constant: SGreedy$^{\mathrm{d}}$

(d) stability constant: random $\{x_m^{\mathrm{c}}\}$

Figure 16. Behavior of the error and stability constant as a function of M and N for two different set of observation points ($\tilde{\mu} = 0.921$).

2. M. Barrault, Y. Maday, N. C. Nguyen, and A. T. Patera. An "empirical interpolation" method: application to efficient reduced-basis discretization of partial differential equations. *C. R. Acad. Sci. Paris, Ser. I*, 339:667–672, 2004.

3. P. Binev, A. Cohen, W. Dahmen, R. DeVore, G. Petrova, and P. Wojtaszczyk. Convergence rates for greedy algorithms in reduced basis methods. *SIAM J. Math. Anal.*, 43:1457–1472, 2011.

4. A. Buffa, Y. Maday, A. T. Patera, C. Prud'homme, and G. Turinici. A priori convergence of the greedy algorithm for the parametrized reduced basis method. *Math. Model. Numer. Anal.*, 46:595–603, 2012.

5. G. Chardon, A. Cohen, and L. Daudet. Sampling and reconstruction of solutions to the Helmholtz equation. *Sampling Theory in Signal and Image Processing*, page submitted, 2013.

6. A. Cohen, M. Davenport, and D. Leviatan. On the stability and accuracy of least-squares approximations. *Fond. Comput. Math.*, 13:819–834, 2013.

7. R. DeVore, G. Petrova, and P. Wojtaszczyk. Greedy algorithms for reduced basis in Banach spaces. *Constructive Approximation*, 37:455–466, 2013.

8. R. Everson and L. Sirovich. Karhunen-Loève procedure for gappy data. *J. Opt. Soc. Am. A*, 12(8):1657–1664, 1995.

9. J. P. Fink and W. C. Rheinboldt. On the error behavior of the reduced basis technique for nonlinear finite element approximations. *ZAMM - Journal of Applied Mathematics and Mechanics / Zeitschrift fr Angewandte Mathematik und Mechanik*, 63(1):21–28, 1983.

10. M. Fisher. Assimilation algorithms. ECMWF NWP-DA Training Course, 2013, Reading, UK.

11. G. Franceschini and S. Macchietto. Model-based design of experiments for parameter precision: state of the art. *Chem. Eng. Sci.*, 63:4846–4872, 2008.

12. U. Hetmaniuk, R. Tezaur, and C. Farhat. An adaptive scheme for a class of interpolatory model reduction methods for frequency response problems. 93, 2013.

13. R. E. Kalman. A new approach to linear filtering and prediction problems. *Transactions of the ASME–Journal of Basic Engineering*, 82(Series D):35–45, 1960.

14. K. Kunisch and S. Volkwein. Galerkin proper orthogonal decomposition methods for parabolic problems. *Numerische Mathematik*, 90(1):117–148, 2001.

15. P. Ladevèze and L. Chamoin. On the verification of model reduction methods based on the proper generalized decomposition. *Comput. Methods Appl. Mech. Engrg.*, 200:2032–2047, 2011.

16. Z. L. Li and I. M. Navon. Optimality of variational data assimilation and its relationship with the Kalman filter and smoother. *Q.J.R. Meteorol*, 127:661–683, 2001.

17. A. C. Lorenc. A global three-dimensional multivariate statistical interpolation scheme. *Mon. Wea. Rev.*, 109:701–721, 1981.

18. Y. Maday and O. Mula. A generalized empirical interpolation method: application of reduced basis techniques to data assimilation. In F. Brezzi, P. C. Franzone, U. Gianazza, and G. Gilardi, editors, *Analysis and numerics of partial differential equations*, pages 221–235. Springer-Verlag, 2013.

19. Y. Maday, A. T. Patera, and D. V. Rovas. A blackbox reduced-basis output bound method for noncoercive linear problems. In D. Cioranescu and J. L. Lions, editors, *Studies in Mathematics and its Applications*, pages 533–569. Elsevier Science B. V., 2002.

20. B. D. Moor. Structured total least squares and l_2 apprximation problems. *Linear Algebra and its Applications*, 188–189:163–205, 1993.

21. N. C. Nguyen and J. Peraire. An interpolation method for the reconstruction and recognition of face images. In A. Ranchordas, H. Araújo, and J. Vitrià, editors, *VISAPP (2)*, pages 91–96. INSTICC - Institute for Systems and Technologies of Information, Control and Communication, 2007.

22. A. T. Patera and E. M. Rønquist. Regression on parametric manifolds: estimation of spatial fields, functional outputs, and parameters from noisy data. *C. R. Acad. Sci. Paris, Ser. I*, 350:543–547, 2012.

23. T. A. Porsching. Estimation of the error in the reduced basis method solution of nonlinear equations. *Math. Comp.*, 45(172):487–496.

24. A. Quarteroni and A. Valli. *Numerical Approximation of Partial Differential Equations*. Springer, New York, 1997.

25. G. Rozza, D. B. P. Huynh, and A. T. Patera. Reduced basis approximation and *a posteriori* error estimation for affinely parametrized elliptic coercive partial differential equations — application to transport and continuum mechanics. *Archives of Computational Methods in Engineering*, 15(3):229–275, 2008.

26. T. Taddai. Private communication, Jan. 2014.

27. K. Willcox. Unsteady flow sensing and estimation via the gappy proper orthogonal decomposition. *Computers & Fluids*, 35(2), 2006.

28. M. Yano, J. D. Penn, and A. T. Patera. A model-data weak formulation for simultaneous estimation of state and bias. *C. R. Acad. Sci. Paris, Ser. I*, accepted, 2013.